Appl. Phys. B 55, 265–278 (1992)

Applied Physics B Photophysics and Laser Chemistry

Realization of the Einstein-Podolsky-Rosen Paradox for Continuous Variables in Nondegenerate Parametric Amplification

Z. Y. Ou, S. F. Pereira, and H. J. Kimble

Norman Bridge Laboratory of Physics 12-33, California Institute of Technology, Pasadena, CA 91125, USA

Received 9 March 1992/Accepted 10 June 1992

Abstract. The Einstein-Podolsky-Rosen (EPR) paradox is demonstrated experimentally for continuous variables by employing a nondegenerate optical parametric amplifier (NOPA). Such a system is analogous to and under some ideal conditions is in one-to-one correspondence with the original system discussed by EPR. In particular, the quadrature-phase amplitudes for a signal beam are inferred in turn from those of a spatially separated but strongly correlated idler beam, where these optical amplitudes are analogous to canonical position and momentum variables. The variances for the two inferences are measured and their product is observed to be below the limit of unity associated with the Heisenberg uncertainty relation, in apparent contradiction with quantum mechanics according to the argument of EPR. The smallest product of inference variances achieved in the experiment is (0.70 ± 0.01). Various other types of quantum noise for this system are also investigated, and a theory of a narrowband NOPA is presented with losses included. A comparison between experiment and this theory shows relatively good agreement. The question of a local hidden-variables description of the system is discussed.

PACS: 42.50

Over the past several years, the process of parametric down-conversion has been employed to produce a variety of nonclassical states of light. Depending on the type of the parametric process considered and on the strength of the pump wave, various groups have generated squeezed states [1–8], single-photon Fock states [9], two-photon states [10] and twin photon beams [11–14] with relative ease in the laboratory. Applications with these nonclassical states in precision measurement [2, 15], spectroscopy [8] and quantum communication [16] have also been explored. For the particular case of nondegenerate parametric down-conversion, the pump photon is split into a pair of photons called signal and idler that are highly correlated in time [17] and in photon number [11–14] (Fig.1a). The quadrature-phase amplitudes for these two beams are also highly correlated as was discussed by Yurke [18] and exploited by La Porta et al. [19] to perform a back-action evasion experiment. Later, Reid and Drummond [20] systematically analyzed a nondegenerate optical parametric oscillator (NOPO) and the correlations between quadrature-phase amplitudes for the signal and idler beams. When the pump beam to the NOPO is relatively strong but below a certain threshold value, this system can be considered as a nondegenerate optical parametric amplifier (NOPA) with appreciable gain over a limited bandwidth. For inputs in the vacuum state, the OPA amplifies the incoming vacuum noise and produces two noisy outgoing signal and idler beams with large fluctuations in quadrature-phase amplitudes. However, because of the splitting of the pump photons in the amplification process, the fluctuations of optical amplitudes for the two beams are strongly correlated

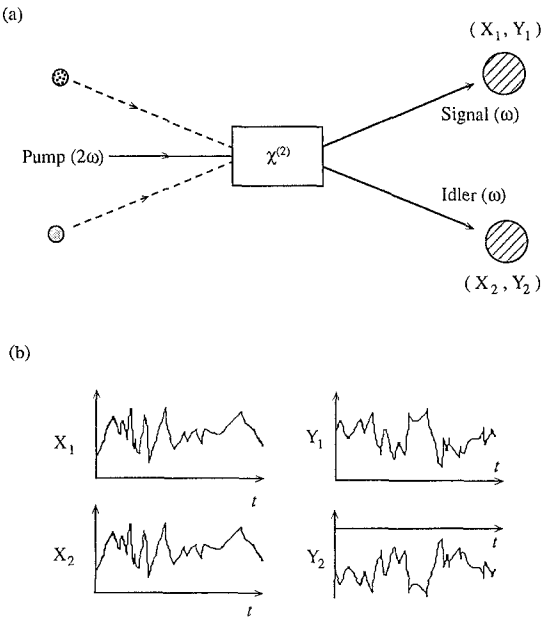

Fig. 1. a Nondegenerate parametric down-conversion via the second-order susceptibility $\chi^{(2)}$. **b** Schematic representation of the fluctuating field amplitudes in the output from a NOPA showing the correlations between the quadrature-phase amplitudes (X_1, Y_1) of the signal beam and (X_2, Y_2) of the idler beam

so that under a limiting condition, they can become "quantum copies" of each other (Fig.lb). It is this type of nonclassical correlation of quadrature-phase amplitudes of the two spatially separated signal and idler beams that led Reid and Drummond [20, 21] to suggest a possible avenue to demonstrate the original Einstein-Podolsky-Rosen paradox in quantum theory.

Recall that in 1935, Einstein, Podolsky and Rosen (EPR) [22] proposed a gedanken experiment involving a system of two particles spatially separated but correlated in position and momentum. From their view of local realism, EPR concluded that quantum mechanics is incomplete since apparently canonically conjugate variables for one of the particles could be assigned definite values from measurements of the other particle in conflict with the Heisenberg uncertainty principle [23]. Subsequently, Bohm [24] presented a variant of EPR's argument for a system of discrete variables and analyzed [25] an experiment performed by Wu and Saharov [26]. The irreducible conflict between quantum mechanics and local realism was finally understood and formalized by Bell in the well-known Bell inequalities [27, 28]. Since then there have been numerous discussions and experiments related to this issue, with a very persuasive experiment being the one by Aspect et al. [29]. Note that throughout the second half of this century, most theoretical discussions including the classic one by Bell and all experimental demonstrations have focused on Bohm's version of the EPR paradox which involves a system with discrete variables (such as electron spin or photon polarization), in contrast to the system originally discussed by EPR with continuous variables (position and momentum).

The fundamental issue in experiments of the type proposed either by EPR or by Bohm is the existence in quantum theory of a kind of nonlocal correlation between two spatially separated subsystems. Of course Bell [27] proved that such quantum correlations are so large in certain systems as to exclude a whole class of theories based upon objective realism (the so called hidden-variables theories). Returning to the example of signal and idler beams generated by parametric down conversion, we might expect that the strong intrinsic correlations of these beams could lead to the kind of quantum nonlocal correlations discussed above. This is indeed the case as has been demonstrated in experiments involving fourth-order interference of signal and idler beams where Bohm's argument applies to the polarization correlations of a suitably arranged system and where violations of Bell inequalities have been reported [30, 31]. Other fourth-order interference experiments demonstrating quantum nonlocal correlations have involved such variables as position [32] and phase [33]. However, there does not exist a position observable for the photon [34] and experiments parametrized by phase delay as in [33] lead to discrete outcomes and to Bell inequalities with the same form as those for polarizations [31]. In any case many recent observations involving fourth-order interference are directed to the question of Einstein locality and not to the explicit demonstration of the EPR paradox.

Inclusive of these experiments with photon pairs in parametric down conversion, the reported demonstrations of the EPR paradox and of violations of Bell inequalities are based on correlations of discrete variables. As far as we know, an experimental demonstration of the EPR paradox with continuous variables along the lines of the original discussion has not yet been realized either optically or otherwise. Possible demonstrations of the original EPR paradox by employing the scattering of massive particles [25] are hampered by the requirements for extremely accurate measurements of the positions and momenta of the particles after the scattering event. By contrast it is relatively straightfoward to implement a nearly ideal measurement of quadrature-phase amplitudes of an optical field. Hence the nonclassical correlations of quadrature-phase amplitudes studied by Reid and Drummond [20] and by Reid [21] for the system of two spatially separated signal and idler beams produced in nondegenerate parametric amplification provide an extremely attractive avenue toward a realization of the original EPR gedanken experiment. Actually, in the limiting case when the parametric gain approaches infinity and passive losses go to zero, the wave function for the state of signal and idler modes has the same form as the wave function for the two particles discussed by EPR (see Sect. 2). More specifically, each mode of the electromagnetic field is analogous to a harmonic oscillator, with the quadrature-phase amplitudes of the electromagnetic field playing the roles of canonical position and momentum variables for the oscillator. Since quadrature-phase amplitudes of light can be readily measured with a homodyne detection scheme, the demonstration of the original EPR paradox becomes feasible.

We should however note at the outset that the correlations originally discussed by EPR can be described in purely local terms with the aid of the Wigner function [35, 36]. Since the Wigner function is everywhere positive both for the original EPR gedanken experiment as well as for the experiment that we report, we must conclude that the EPR correlations are not in conflict with local realism and that no paradox exists in the modern sense (i.e., there is a local hidden variable theory that successfully describes the system [36]). By contrast, the nonlocal correlation for the spin and polarization systems is irreducible as specified by the Bell inequalities [27, 28]. Thus the demonstration of the original EPR paradox does not enable us to say anything about local realism and quantum theory. Nonetheless, an investigation of correlations of continuous variables in spatially extended systems is a first step toward a possible generalization of the Bell inequalities to this setting.

In this paper, we study the nonclassical correlations of quadrature-phase amplitudes between signal and idler beams generated by a subthreshold optical parametric oscillator that is operated in a frequency degenerate but polarization nondegenerate mode. By inferring in turn the two quadrature-phase amplitudes of the signal beam from measurements of those of the spatially separated idler beam, we are able to achieve a reasonably faithful realization of the original EPR paradox with continuous variables. If instead of directly examining the signal and idler modes, these fields are combined to form two new modes, we find that both of these new modes are squeezed and exhibit noise reduction below the vacuum noise level. The measured correlations and noise reductions are compared with a theoretical treatment similar to that in [20] with good agreement.

The organization of the paper is as follows: in Sect. 1, we present a theoretical treatment of a nondegenerate optical

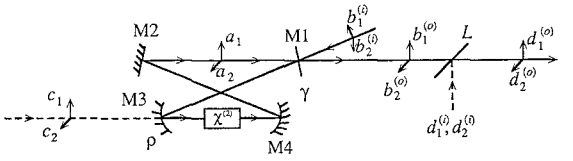

Fig. 2. Geometry of the nondegenerate optical parametric amplifier (NOPA) for the theoretical analysis

parametric oscillator below threshold. The treatment follows the input-output formalism of Collett and Gardiner [37a] and includes both internal and external losses of the NOPA. We calculate in particular the relevant measurable quantities for our experiment. Section 2 is devoted to an analysis of the demonstration of the EPR paradox for continuous variables with less than ideal correlations. The Wigner function for the NOPA is also derived. The actual experiment involving a subthreshold OPO and two sets of balanced homodyne detectors is discussed in Sect. 3. We conclude in Sect. 4 with a summary of our results, a discussion about the hidden-variables description of the NOPA, and with a brief description of a quantum communication experiment that utilizes the correlation properties of the NOPA.

1 Theoretical Treatment of the NOPA

The system that we consider consists of a two-ended optical cavity with two modes a_1, a_2 and a nonlinear medium characterized by the nonlinear susceptibility $\chi^{(2)}$ which provides for an interaction between two modes (Fig. 2). The two modes are orthogonally polarized but may be degenerate in frequency. For simplicity here, we will assume that both modes experience the same loss inside the cavity as well as outside the cavity. The internal losses of the system are modeled as leakage via a mirror at one end of the cavity with damping rate ϱ. We denote by c_1, c_2 the unwanted vacuum modes that are coupled into the cavity through the leakage loss at mirror $M3$. The fields of interest are coupled in and out through the mirror $M1$, which is characterized by the damping rate γ that is assumed to be the same for both modes. The input and output fields are denoted by $b_1^{(\mathrm{i})}, b_2^{(\mathrm{i})}$ and $b_1^{(\mathrm{o})}, b_2^{(\mathrm{o})}$, respectively. In the limit of weak coupling, we take the Hamiltonian for this system to be given by [37, 38]

$$H = H_\mathrm{S} + H_\mathrm{I} + H_\mathrm{R} + H_\mathrm{SR}\,, \tag{1}$$

where

$$H_\mathrm{I} = \mathrm{i}\hbar\kappa(a_1^\dagger a_2^\dagger\,\mathrm{e}^{-2\mathrm{i}\omega_0 t} - a_1 a_2\,\mathrm{e}^{2\mathrm{i}\omega_0 t}) \tag{2}$$

is the interaction Hamiltonian describing the coupling between the modes $a_{1,2}$. Note that we assume that the nonlinear medium is pumped by a field in a coherent state of frequency $2\omega_0$ and that the pump field is undepleted and described by a c-number which is included in the coupling coefficient κ. We will take κ to be real without the loss of generality. The Hamiltonian for the two (internal) cavity modes of resonant frequencies (ω_1, ω_2) is

$$H_\mathrm{S} = \hbar\omega_1 a_1^\dagger a_1 + \hbar\omega_2 a_2^\dagger a_2\,, \tag{3}$$

with a similar expression for H_R, which is the Hamiltonian for the external modes. H_SR is the Hamiltonian that describes the coupling of the internal modes $(a_{1,2})$ to the modes $(b_{1,2}^{(\mathrm{i,o})}, c_{1,2})$ external to the cavity, and accounts for the excitation and decay of the internal modes.

Following the formalism of Collett and Gardiner [37a], we derive equations of motion for the two cavity modes a_1, a_2 as

$$\begin{aligned}\frac{da_1}{dt} &= -\mathrm{i}\omega_1 a_1 + \kappa\mathrm{e}^{-2\mathrm{i}\omega_0 t}a_2^\dagger \\ &\quad - \frac{\gamma+\varrho}{2}\,a_1 + \sqrt{\gamma}b_1^{(\mathrm{i})} + \sqrt{\varrho}c_1\,, \\ \frac{da_2}{dt} &= -\mathrm{i}\omega_2 a_2 + \kappa\mathrm{e}^{-2\mathrm{i}\omega_0 t}a_1^\dagger \\ &\quad - \frac{\gamma+\varrho}{2}\,a_2 + \sqrt{\gamma}b_2^{(\mathrm{i})} + \sqrt{\varrho}c_2\,.\end{aligned} \tag{4}$$

The output quantities $b_{1,2}^{(\mathrm{o})}$ then follow from the boundary conditions

$$b_{1,2}^{(\mathrm{o})} + b_{1,2}^{(\mathrm{i})} = \sqrt{\gamma}a_{1,2}\,. \tag{5}$$

In order to solve (4, 5), we first move to a rotating frame at frequency ω_0 by setting

$$o(t) \equiv O(t)\mathrm{e}^{-\mathrm{i}\omega_0 t} \tag{6}$$

with $o = [a_{1,2}; b_{1,2}^{(\mathrm{i,o})}; c_{1,2}]$ and $O = [A_{1,2}; B_{1,2}^{(\mathrm{i,o})}; C_{1,2}]$, and then make the Fourier transformation

$$O(\Omega) = \frac{1}{\sqrt{2\pi}}\int \mathrm{d}t\, O(t)\mathrm{e}^{-\mathrm{i}\Omega t}\,, \tag{7}$$

with commutation relation $[O(\Omega), O^\dagger(\Omega')] = \delta(\Omega - \Omega')$ for $B_{1,2}^{(\mathrm{i,o})}$, $C_{1,2}$. From (4–7), after some straightforward algebra, we can relate the output quantities to the input quantities as follows

$$\begin{aligned}B_j^{(\mathrm{o})}(\Omega) &= \frac{\{\kappa^2 + [(\gamma-\varrho)/2 + \mathrm{i}(\Omega+\Delta_j)]\,[(\gamma+\varrho)/2 - \mathrm{i}(\Omega-\Delta_k)]\}B_j^{(\mathrm{i})}(\Omega)}{[(\gamma+\varrho)/2 - \mathrm{i}(\Omega+\Delta_j)]\,[(\gamma+\varrho)/2 - \mathrm{i}(\Omega-\Delta_k)] - \kappa^2} \\ &\quad + \frac{\kappa\gamma B_k^{(\mathrm{i})\dagger}(-\Omega) + [(\gamma+\varrho)/2 - \mathrm{i}(\Omega-\Delta_k)]\sqrt{\gamma\varrho}C_j(\Omega) + \kappa\sqrt{\gamma\varrho}C_k^\dagger(-\Omega)}{[(\gamma+\varrho)/2 - \mathrm{i}(\Omega+\Delta_j)]\,[(\gamma+\varrho)/2 - \mathrm{i}(\Omega-\Delta_k)] - \kappa^2}\,,\end{aligned} \tag{8}$$

where $j = 1$, $k = 2$ or vice versa, and $\Delta_{1,2} = \omega_0 - \omega_{1,2}$. From now on, let us assume that the two cavity modes are frequency degenerate and on resonance with ω_0 so that $\Delta_{1,2} = 0$. Then (8) can be simplified to

$$\begin{aligned}B_j^{(\mathrm{o})}(\Omega) &= G(\Omega)B_j^{(\mathrm{i})}(\Omega) + g(\Omega)B_k^{(\mathrm{i})\dagger}(-\Omega) \\ &\quad + \bar{G}(\Omega)C_j(\Omega) + \bar{g}(\Omega)C_k^\dagger(-\Omega)\end{aligned} \tag{9}$$

with

$$\begin{aligned}G(\Omega) &= \{\kappa^2 + [(\gamma-\varrho)/2 + \mathrm{i}\Omega]\,[(\gamma+\varrho)/2 - \mathrm{i}\Omega]\}/M \\ &= G^*(-\Omega)\,, \\ g(\Omega) &= \kappa\gamma/M = g^*(-\Omega)\,, \\ \bar{G}(\Omega) &= [(\gamma+\varrho)/2 - \mathrm{i}\Omega]\sqrt{\gamma\varrho}/M = \bar{G}^*(-\Omega)\,, \\ \bar{g}(\Omega) &= \kappa\sqrt{\gamma\varrho}/M = \bar{g}^*(-\Omega)\,,\end{aligned} \tag{10}$$

where $M \equiv [(\gamma+\varrho)/2 - \mathrm{i}\Omega]^2 - \kappa^2$. If the inputs to the cavity are in a vacuum state (as will be assumed throughout this paper), then

$$\begin{aligned}
&\langle B_j^{(\mathrm{o})\dagger}(\Omega) B_j^{(\mathrm{o})}(\Omega')\rangle = [|g(\Omega)|^2 + |\bar{g}(\Omega)|^2]\delta(\Omega-\Omega')\,,\\
&\langle B_j^{(\mathrm{o})}(\Omega) B_j^{(\mathrm{o})\dagger}(\Omega')\rangle = [|G(\Omega)|^2 + |\bar{G}(\Omega)|^2]\delta(\Omega-\Omega')\,,\\
&\langle B_j^{(\mathrm{o})}(\Omega) B_k^{(\mathrm{o})}(\Omega')\rangle\\
&\quad = [G(\Omega)g^*(\Omega) + \bar{G}(\Omega)\bar{g}^*(\Omega)]\delta(\Omega+\Omega')\,,
\end{aligned} \tag{11}$$

with $\{j,k\} = \{1,2\}, \{2,1\}$. The other averages for the external modes are zero.

Let us now introduce external losses for the output modes $B_{1,2}^{(\mathrm{o})}$ by using a beamsplitter model with uncorrelated vacuum modes $D_1^{(\mathrm{i})}, D_2^{(\mathrm{i})}$ from one of the ports (Fig. 2). If the total external loss is denoted as L, then we find the detected fields $D_1^{(\mathrm{o})}$, $D_2^{(\mathrm{o})}$ as

$$D_{1,2}^{(\mathrm{o})}(\Omega) = \sqrt{1-L}\,B_{1,2}^{(\mathrm{o})}(\Omega) + \mathrm{i}\sqrt{L}\,D_{1,2}^{(\mathrm{i})} \tag{12}$$

In this simple model, the total external loss L is meant to include propagation loss as well as the non-unit homodyne efficiencies and quantum efficiencies of the detectors.

With (9–12) we can calculate various measurable quantities. But before doing that, let us first examine some special cases in order to reveal the physics which is otherwise masked by complicated algebraic expressions. To do so, we assume that the system is lossless so that $L = \varrho = 0$. Then we have

$$\left.\begin{aligned}
&D_{1,2}^{(\mathrm{o})}(\Omega) = G(\Omega)B_{1,2}^{(\mathrm{i})}(\Omega) + g(\Omega)B_{2,1}^{(\mathrm{i})\dagger}(-\Omega)\,,\\
&\text{where}\\
&G(\Omega) = (\kappa^2 + \gamma^2/4 + \Omega^2)/[(\gamma/2 - \mathrm{i}\Omega)^2 - \kappa^2]\,,\\
&g(\Omega) = \kappa\gamma/[(\gamma/2 - \mathrm{i}\Omega)^2 - \kappa^2]\,,
\end{aligned}\right\} \tag{13}$$

with

$$|G(\Omega)|^2 - |g(\Omega)|^2 = 1\,.$$

These are just the familiar input-output relations for a lossless nondegenerate parametric amplifier of finite bandwidth. The gain of the amplifier depends on the pump strength and can be extremely large as the threshold of the system is approached ($\kappa \to \gamma/2$) and $\Omega \to 0$. If we introduce the quadrature-phase amplitudes defined as

$$\left.\begin{aligned}
X_{1,2}(\Omega) &= D_{1,2}^{(\mathrm{o})}(\Omega) + D_{1,2}^{(\mathrm{o})\dagger}(-\Omega)\,,\\
Y_{1,2}(\Omega) &= D_{1,2}^{(\mathrm{o})}(\Omega)\mathrm{e}^{-\mathrm{i}\pi/2} + D_{1,2}^{(\mathrm{o})\dagger}(-\Omega)\mathrm{e}^{\mathrm{i}\pi/2}\,,\\
X_{1,2}^{(\mathrm{i})}(\Omega) &= B_{1,2}^{(\mathrm{i})}(\Omega) + B_{1,2}^{(\mathrm{i})\dagger}(-\Omega)\,,\\
Y_{1,2}^{(\mathrm{i})}(\Omega) &= B_{1,2}^{(\mathrm{i})}(\Omega)\mathrm{e}^{-\mathrm{i}\pi/2} + B_{1,2}^{(\mathrm{i})\dagger}(-\Omega)\mathrm{e}^{\mathrm{i}\pi/2}\,,
\end{aligned}\right\} \tag{14}$$

then (13) are transformed to

$$\left.\begin{aligned}
X_{1,2}(\Omega) &= G(\Omega)X_{1,2}^{(\mathrm{i})}(\Omega) + g(\Omega)X_{2,1}^{(\mathrm{i})}(\Omega)\,,\\
Y_{1,2}(\Omega) &= G(\Omega)Y_{1,2}^{(\mathrm{i})}(\Omega) - g(\Omega)Y_{2,1}^{(\mathrm{i})}(\Omega)\,.
\end{aligned}\right\} \tag{15}$$

Let us now define a new set of modes $(\bar{D}_1, \bar{D}_2)$, $(\bar{B}_1^{(\mathrm{i})}, \bar{B}_2^{(\mathrm{i})})$ formed from superpositions of the original modes $(D_1^{(\mathrm{o})}, D_2^{(\mathrm{o})})$, $(B_1^{(\mathrm{i})}, B_2^{(\mathrm{i})})$:

$$\left.\begin{aligned}
\bar{B}_1^{(\mathrm{i})} &= \frac{B_1^{(\mathrm{i})} + B_2^{(\mathrm{i})}}{\sqrt{2}}\,, \qquad \bar{B}_2^{(\mathrm{i})} = \frac{B_1^{(\mathrm{i})} - B_2^{(\mathrm{i})}}{\sqrt{2}}\,;\\
\bar{D}_1^{(\mathrm{o})} &= \frac{D_1^{(\mathrm{o})} + D_2^{(\mathrm{o})}}{\sqrt{2}}\,, \qquad \bar{D}_2^{(\mathrm{o})} = \frac{D_1^{(\mathrm{o})} - D_2^{(\mathrm{o})}}{\sqrt{2}}\,.
\end{aligned}\right\} \tag{16}$$

Then (13) become

$$\left.\begin{aligned}
\bar{D}_1^{(\mathrm{o})} &= G(\Omega)\bar{B}_1^{(\mathrm{i})}(\Omega) + g(\Omega)\bar{B}_1^{(\mathrm{i})\dagger}(-\Omega)\,,\\
\bar{D}_2^{(\mathrm{o})} &= G(\Omega)\bar{B}_2^{(\mathrm{i})}(\Omega) - g(\Omega)\bar{B}_2^{(\mathrm{i})\dagger}(-\Omega)\,,
\end{aligned}\right\} \tag{17}$$

which are the equations for two *independent* degenerate parametric amplifiers. Thus the originally coupled two modes $(D_1^{(\mathrm{o})}, D_2^{(\mathrm{o})})$ are transformed into two independent modes $(\bar{D}_1^{(\mathrm{o})}, \bar{D}_2^{(\mathrm{o})})$, which are individually (and independently) in squeezed states. The spectra of squeezing for the two decoupled modes can be easily calculated from (17) and have the following (non-normally ordered) forms:

$$\left.\begin{aligned}
&\langle \bar{X}_1(\Omega)\bar{X}_1(\Omega')\rangle\\
&\quad = \delta(\Omega+\Omega')S_+(\Omega) = \langle \bar{Y}_2(\Omega)\bar{Y}_2(\Omega')\rangle\,,\\
&\langle \bar{Y}_1(\Omega)\bar{Y}_1(\Omega')\rangle\\
&\quad = \delta(\Omega+\Omega')S_-(\Omega) = \langle \bar{X}_2(\Omega)\bar{X}_2(\Omega')\rangle\,,
\end{aligned}\right\} \tag{18}$$

with

$$\begin{aligned}
S_+(\Omega) &= |G(\Omega) + g(\Omega)|^2 = 1 + 2\kappa\gamma/[(\kappa-\gamma/2)^2 + \Omega^2]\,,\\
S_-(\Omega) &= |G(\Omega) - g(\Omega)|^2 = 1 - 2\kappa\gamma/[(\kappa+\gamma/2)^2 + \Omega^2]\,.
\end{aligned}$$

On the other hand, from (15), the quadrature-phase amplitudes of the original signal and idler modes $(D_1^{(\mathrm{o})}, D_2^{(\mathrm{o})})$ defined in (14) have variances of the following form:

$$\left.\begin{aligned}
\langle X_1(\Omega)X_1(\Omega')\rangle &= \delta(\Omega+\Omega')T_1^X(\Omega)\,,\\
\langle Y_1(\Omega)Y_1(\Omega')\rangle &= \delta(\Omega+\Omega')T_1^Y(\Omega)\,,\\
\langle X_2(\Omega)X_2(\Omega')\rangle &= \delta(\Omega+\Omega')T_2^X(\Omega)\,,\\
\langle Y_2(\Omega)Y_2(\Omega')\rangle &= \delta(\Omega+\Omega')T_2^Y(\Omega)\,,
\end{aligned}\right\} \tag{19}$$

where $T_1^X(\Omega) = T_2^X(\Omega) = T_1^Y(\Omega) = T_2^Y(\Omega) \equiv G_{\mathrm{q}}(\Omega)$. Here the quantum noise gain $G_{\mathrm{q}}(\Omega)$ is given by

$$\begin{aligned}
G_{\mathrm{q}}(\Omega) &= |G(\Omega)|^2 + |g(\Omega)|^2\\
&= \frac{(\gamma^2/4 + \kappa^2 + \Omega^2)^2 + \gamma^2\kappa^2}{(\gamma^2/4 - \kappa^2 - \Omega^2)^2 + \gamma^2\Omega^2}
\end{aligned} \tag{20}$$

and describes the phase-insensitive fluctuations of the signal $(D_1^{(\mathrm{o})})$ and idler $(D_2^{(\mathrm{o})})$ outputs of the system. Note that $G_{\mathrm{q}}(\Omega) \to \infty$ as $\kappa \to \gamma/2 \equiv \kappa_{\mathrm{th}}$ and $\Omega \to 0$. Therefore, from the above equations we see that the system amplifies the vacuum noises of the inputs $(B_{1,2}^{(\mathrm{i})})$ and generates two outputs with large noises $(D_{1,2}^{(\mathrm{o})})$. However, the difference of the X amplitudes is such that

$$\left.\begin{aligned}
&X_1(\Omega) - X_2(\Omega)\\
&\quad = [G(\Omega) - g(\Omega)]\,[X_1^{(\mathrm{i})}(\Omega) - X_2^{(\mathrm{i})}(\Omega)]\\
&\quad = \frac{\kappa - \gamma/2 + \mathrm{i}\Omega}{\kappa + \gamma/2 - \mathrm{i}\Omega}\,[X_1^{(\mathrm{i})}(\Omega) - X_2^{(\mathrm{i})}(\Omega)]\\
&\quad \to 0 \quad \text{as} \quad \kappa \to \gamma/2 \quad \text{and} \quad \Omega \to 0\,,
\end{aligned}\right\} \tag{21a}$$

while the sum of the Y amplitudes is

$$\left.\begin{aligned} &Y_1(\Omega)+Y_2(\Omega)\\ &=[G(\Omega)-g(\Omega)]\,[Y_1^{(\mathrm{i})}(\Omega)+Y_2^{(\mathrm{i})}(\Omega)]\\ &=\frac{\kappa-\gamma/2+\mathrm{i}\Omega}{\kappa+\gamma/2-\mathrm{i}\Omega}\,[Y_1^{(\mathrm{i})}(\Omega)+Y_2^{(\mathrm{i})}(\Omega)]\\ &\quad\to 0\quad\text{as}\quad\kappa\to\gamma/2\quad\text{and}\quad\Omega\to 0\,, \end{aligned}\right\} \tag{21b}$$

indicating that the two outputs $(b_{1,2}^{(\mathrm{o})})$ are highly correlated. Actually, if we set $\kappa=\gamma/2$ and $\Omega=0$, then

$$\left.\begin{aligned} &X_1(0)=X_2(0)\,,\\ &Y_1(0)=-Y_2(0)\,, \end{aligned}\right\} \tag{22}$$

and the quadrature-phase amplitudes of the output beams become "quantum copies" of one another since (22) is an operator equation.

To quantify the degree of the correlation, we introduce the spectral variances $V_{\pm}(\Omega)$ given by

$$\begin{aligned} &\langle[Y_1(\Omega)+Y_2(\Omega)]\,[Y_1(\Omega')+Y_2(\Omega')]\rangle\\ &\quad=\delta(\Omega+\Omega')V_+(\Omega)\,,\\ &\langle[X_1(\Omega)-X_2(\Omega)]\,[X_1(\Omega')-X_2(\Omega')]\rangle\\ &\quad=\delta(\Omega+\Omega')V_-(\Omega)\,, \end{aligned} \tag{23}$$

where from (18)

$$V_+(\Omega)=V_-(\Omega)=2S_-=2\,\frac{(\kappa-\gamma/2)^2+\Omega^2}{(\kappa+\gamma/2)^2+\Omega^2}\,. \tag{24}$$

Note that the factor 2 can be traced to the contributions of the uncorrelated vacuum fluctuations of the input modes $B_{1,2}^{(\mathrm{i})}$ (21a, b). This is obvious when we set $\kappa=0$ in (24) which corresponds to unit gain for the system and thus vacuum fields for $D_{1,2}^{(\mathrm{o})}$; in this case, $V_{\pm}(\Omega)=2$. On the other hand, when $\kappa=\gamma/2$ and $\Omega=0$ (so that $G\to\infty$), we find that $V_{\pm}(0)=0$, corresponding to perfect correlation.

In practice of course, the gain of the system is not infinite, and in this case $X_1(\Omega)$ $[Y_1(\Omega)]$ are better correlated to the scaled quantities $\lambda X_2(\Omega)$ $[-\lambda Y_2(\Omega)]$, with $0\le\lambda<1$ properly adjusted for best correlation [21]. Hence the quantities $V_{\pm}^{\lambda}(\Omega)$ defined as

$$\left.\begin{aligned} &\langle[X_1(\Omega)-\lambda X_2(\Omega)]\,[X_1(\Omega')-\lambda X_2(\Omega')]\rangle\\ &\quad=\delta(\Omega+\Omega')V_-^{\lambda}(\Omega)\,,\\ &\langle[Y_1(\Omega)+\lambda Y_2(\Omega)]\,[Y_1(\Omega')+\lambda Y_2(\Omega')]\rangle\\ &\quad=\delta(\Omega+\Omega')V_+^{\lambda}(\Omega)\,, \end{aligned}\right\} \tag{25}$$

offer an alternative statement of the degree of correlation between modes 1 and 2. As we shall soon see, the quantities $V_{\pm}^{\lambda}(\Omega)$ will better serve our investigation of EPR correlations since $V_{\pm}^{\lambda}(\Omega)$ are always smaller than $V_{\pm}(\Omega)$. Explicitly from (15) we have that

$$V_{\pm}^{\lambda}(\Omega)=\frac{(\gamma^2/4-\kappa^2-\Omega^2)^2+\gamma^2\Omega^2}{(\gamma^2/4+\kappa^2+\Omega^2)^2+\gamma^2\kappa^2}\le V_{\pm}(\Omega)\,, \tag{26}$$

where λ has been chosen to minimize $V_{\pm}^{\lambda}(\Omega)$.

Returning now to the actual case of finite losses in the system with $(L,\varrho)\neq 0$, we can still introduce the transformation in (16) to find that the two modes $D_{1,2}^{(\mathrm{o})}$ are decoupled into two independent degenerate parametric amplifiers (with the same gain and loss parameters). Following the analysis that lead to (18–20, 26) but with more algebra, we can thus calculate the spectra of squeezing $S_{\pm}(\Omega)$ for the modes $\bar{D}_{1,2}^{(\mathrm{o})}$, the phase-insensitive quantum noise gain $G_{\mathrm{q}}(\Omega)$ for the signal and idler fields $D_{1,2}^{(\mathrm{o})}$, and the correlation quantities $V_{\pm}^{\lambda}(\Omega)$ between the quadrature-phase amplitudes (X_1,Y_1) and (X_2,Y_2). They have the following form:

$$S_+(\Omega)=1+\frac{2(1-L)\kappa\gamma}{[\kappa-(\gamma+\varrho)/2]^2+\Omega^2}\,, \tag{27a}$$

$$S_-(\Omega)=1-\frac{2(1-L)\kappa\gamma}{[\kappa+(\gamma+\varrho)/2]^2+\Omega^2}\,, \tag{27b}$$

$$G_{\mathrm{q}}(\Omega)=1+2(1-L)\kappa^2\gamma(\gamma+\varrho)/|M|^2\,, \tag{27c}$$

$$V_{\pm}^{\lambda}(\Omega)=\frac{1+4(1-L)\kappa^2\gamma(\varrho+L\gamma)/|M|^2}{1+2(1-L)\kappa^2\gamma(\varrho+\gamma)/|M|^2}\,, \tag{27d}$$

where $|M|^2\equiv\Omega^2(\varrho+\gamma)^2+[(\gamma+\varrho)^2/4-\Omega^2-|\kappa|^2]^2$. It is straightforward to check that the results in (27a–d) are same as those in (18–20, 26) when we set all the losses to zero.

Of course, beyond the specific set $(X_{1,2},Y_{1,2})$ of quadrature-phase amplitudes is a continuous set given by

$$\begin{aligned} X_1(\Omega,\phi_1)&=D_1(\Omega)\mathrm{e}^{-\mathrm{i}\phi_1}+D_1^{\dagger}(-\Omega)\mathrm{e}^{\mathrm{i}\phi_1}\,,\\ X_2(\Omega,\phi_2)&=D_2(\Omega)\mathrm{e}^{-\mathrm{i}\phi_2}+D_2^{\dagger}(-\Omega)\mathrm{e}^{\mathrm{i}\phi_2}\,, \end{aligned} \tag{28}$$

which are parametrized by the phases ϕ_1,ϕ_2 for the signal and idler beams, respectively. The quantities $X_{1,2}(\Omega)$, $Y_{1,2}(\Omega)$ are special cases of $X_{1,2}(\Omega,\phi_{1,2})$ when $\phi_{1,2}=0$ and $\pi/2$, respectively, where the phase reference for these choices is specified by our choice of phase for κ (real). A derivation similar to that for (27a–d) leads to the spectra $S_{1,2}(\Omega,\phi_{1,2})$, $T_{1,2}(\Omega,\phi_{1,2})$, and $V_{12}^{\lambda}(\Omega,\phi_1,\phi_2)$ which are associated with $\bar{X}_{1,2}(\Omega,\phi_{1,2})$ (quadrature-phase amplitudes for $\pm45°$ modes), $X_{1,2}(\Omega,\phi_{1,2})$ (quadrature-phase amplitudes for signal and idler modes), and $X_1(\Omega,\phi_1)-\lambda X_2(\Omega,\phi_2)$ (correlation of signal and idler amplitudes), respectively. These quantities are given by

$$\begin{aligned} &S_{1,2}(\Omega,\phi_{1,2})\\ &\quad=S_-(\Omega)+\frac{2(1-L)\kappa\gamma[\kappa^2+(\varrho+\gamma)^2+\Omega^2]}{|M|^2}\\ &\qquad\times(1\pm\cos 2\phi_{1,2})\,, \end{aligned} \tag{29a}$$

$$T_1(\Omega,\phi_1)=T_2(\Omega,\phi_2)=G_{\mathrm{q}}(\Omega)\,, \tag{29b}$$

and

$$\begin{aligned} &\langle[X_1(\Omega,\phi_1)-\lambda X_2(\Omega,\phi_2)]\,[X_1(\Omega',\phi_1)-\lambda X_2(\Omega',\phi_2)]\rangle\\ &\quad\equiv\delta(\Omega+\Omega')V_{12}^{\lambda}(\Omega,\phi_1,\phi_2)\,, \end{aligned}$$

where

$$\begin{aligned} &V_{12}^{\lambda}(\Omega,\phi_1,\phi_2)\\ &\quad=V_{\pm}^{\lambda}(\Omega)\\ &\qquad+\frac{8(1-L)^2\kappa^2\gamma^2[\kappa^2+(\gamma+\varrho)^2/4+\Omega^2]^2/|M|^4}{1+2(1-L)^2\kappa^2\gamma(\gamma+\varrho)/|M|^2}\\ &\qquad\times[1-\cos(\phi_1+\phi_2)]\,. \end{aligned} \tag{29c}$$

It can be easily seen that

$$S_1(\Omega,0) = S_2(\Omega,\pi/2) = S_+(\Omega)\,, \tag{30a}$$

$$S_1(\Omega,\pi/2) = S_2(\Omega,0) = S_-(\Omega)\,, \tag{30b}$$

$$V_{12}^{\lambda}(\Omega,0,0) = V_-^{\lambda}(\Omega) = V_+^{\lambda}(\Omega) = V_{12}^{\lambda}(\Omega,-\pi/2,\pi/2)\,. \tag{30c}$$

In (29c, 30c), λ is chosen such that $V_{\pm}^{\lambda}(\Omega)$ are minimized.

For subsequent comparison with the experimental data, we need to relate the quantities γ, ϱ and Ω, κ to measured quantities. Let us rewrite (27a–d) in terms of the following variables:

$$\left.\begin{aligned} &\varepsilon \equiv 2\kappa/(\varrho+\gamma) \qquad \omega \equiv \frac{2\Omega}{\varrho+\gamma}\,,\\ &L_{\text{overall}} \equiv 1-(1-L)\frac{\gamma}{\gamma+\varrho}\,. \end{aligned}\right\} \tag{31}$$

Then (27a–d) become:

$$S_-(\Omega) = 1 - \frac{4(1-L_{\text{overall}})\varepsilon}{\omega^2+(1+\varepsilon)^2}\,, \tag{32a}$$

$$S_+(\Omega) = 1 - \frac{4(1-L_{\text{overall}})\varepsilon}{\omega^2+(1-\varepsilon)^2}\,, \tag{32b}$$

$$G_{\text{q}}(\Omega) = 1 + 8(1-L_{\text{overall}})\varepsilon^2/\bar{M}^2\,, \tag{32c}$$

$$V_{\pm}^{\lambda}(\Omega) = \frac{1+16L_{\text{overall}}\varepsilon^2(1-L_{\text{overall}})/\bar{M}^2}{1+8(1-L_{\text{overall}})\varepsilon^2/\bar{M}^2}\,, \tag{32d}$$

with $\bar{M}^2 \equiv (\omega^2-1+\varepsilon^2)^2+4\omega^2$. Now (31) can be expressed in terms of readily accessable experimental quantities as follows:

$$\left.\begin{aligned} &\varepsilon = \sqrt{P/P_{\text{th}}}\,,\\ &\omega = (\Omega/2\pi)\frac{2F_{\text{m}}}{\nu_{\text{FSR}}}\,,\\ &L_{\text{overall}} = 1-(1-L)\frac{F_{\text{m}}}{F_{\text{t}}}\,, \end{aligned}\right\} \tag{33}$$

where P is the green pump power with P_{th} as the threshold value. $F_{\text{m}}, F_{\text{t}}$ are the finesses of the NOPA cavity with and without internal losses. F_{m} can be directly measured and F_{t} is calculated from the known transmission of the output coupling mirror M1. ν_{FSR} is the free spectral range of the cavity. The quantities in (32a–d) are exactly the objects of our experimental investigation, which we will discuss in Sect. 3.

2 EPR Paradox and the NOPA

As pointed out by Reid and Drummond [20] and by Reid [21], the correlations between the quadrature-phase amplitudes of the spatially separated signal and idler beams resemble the original correlations discussed by EPR. Indeed, if we go back to (22), we find that the two quadrature-phase amplitudes of mode 1 are identical to those of the mode 2 (with the exception of a sign) under some limiting case. The relationship between the correlations in the NOPA and in the original EPR paper can be best analyzed by comparing their wavefunctions or equivalently their Wigner phase-space functions [35, 36]. With the Wigner functions, we can also address the question of possible local hidden-variable descriptions for these systems.

Towards this end, let us consider the lossless case of NOPA in (13, 15). For the purpose of illustration, we set $\Omega = 0$ and find from (15, 16), that

$$\bar{D}_1 = G\bar{B}_1 + g\bar{B}_1^{\dagger}\,, \qquad \bar{D}_2 = G\bar{B}_2 - g\bar{B}_2^{\dagger}\,, \tag{34}$$

where

$$\left\{\begin{aligned} &G \equiv G(0) \equiv \cosh r\,,\\ &g \equiv g(0) \equiv \sinh r\,, \end{aligned}\right.$$

with $r \geq 0$, and

$$\left\{\begin{aligned} &\bar{D}_{1,2} \equiv \bar{D}_{1,2}^{(\text{o})}(0)\,,\\ &\bar{B}_{1,2} \equiv \bar{B}_{1,2}^{(\text{i})}(0)\,. \end{aligned}\right.$$

For the transformation given in (34), it can be shown that the Wigner function for the modes $\bar{D}_1$, $\bar{D}_2$ is connected to that of modes $\bar{B}_1$, $\bar{B}_2$ by the following simple relations:

$$\left.\begin{aligned} &W_{\bar{D}_1}(\bar{x}_1,\bar{y}_1) = W_{\bar{B}_1}(\mathrm{e}^{-r}\bar{x}_1, \mathrm{e}^{r}\bar{y}_1)\,,\\ &W_{\bar{D}_2}(\bar{x}_2,\bar{y}_2) = W_{\bar{B}_2}(\mathrm{e}^{r}\bar{x}_2, \mathrm{e}^{-r}\bar{y}_2)\,, \end{aligned}\right\} \tag{35}$$

where we can write the Wigner functions for $\bar{D}_1$ and $\bar{D}_2$ separately because they are independent of each other (17). Note that if $\bar{B}_{1,2}$ (or equivalently $B_{1,2}^{(\text{i})}$) are vacuum-state fields, then $W_{\bar{B}_i}(\bar{x}_i,\bar{y}_i)$ $(i=1,2)$ has the simple form

$$W_{\text{vac}}(x,y) = \frac{2}{\pi}\exp[-2(x^2+y^2)]\,, \tag{36}$$

where the variables $(x,y) = (x_i,y_i)$ with $i = 1,2$. The Wigner function for the whole system is then simply the product of the Wigner functions of the two modes $\bar{D}_1$, $\bar{D}_2$, which with (36) becomes

$$\begin{aligned} &W_{\bar{D}_1,\bar{D}_2}(\bar{x}_1,\bar{y}_1;\bar{x}_2,\bar{y}_2)\\ &\quad = W_{\bar{D}_1}(\bar{x}_1,\bar{y}_1)W_{\bar{D}_2}(\bar{x}_2,\bar{y}_2)\\ &\quad = \frac{4}{\pi^2}\exp\{-2(\bar{x}_1^2+\bar{y}_2^2)\mathrm{e}^{-2r} - 2(\bar{x}_2^2+\bar{y}_1^2)\mathrm{e}^{2r}\}\,. \end{aligned} \tag{37}$$

Transferring the above Wigner function for the modes $\bar{D}_1$, $\bar{D}_2$ to that for the modes D_1, D_2 by using (16), we thus have the Wigner function for the signal (D_1) and idler (D_2) modes of the NOPA:

$$\begin{aligned} &W_{D_1,D_2}(x_1,y_1;x_2,y_2)\\ &\quad = \frac{4}{\pi^2}\exp\{-[(x_1+x_2)^2+(y_1-y_2)^2]\mathrm{e}^{-2r}\\ &\qquad - [(x_1-x_2)^2+(y_1+y_2)^2]\mathrm{e}^{2r}\}\,,\\ &\qquad \to C\delta(x_1-x_2)\delta(y_1+y_2) \quad \text{as} \quad r\to\infty\,. \end{aligned} \tag{38}$$

The wavefunction of the system for $\Omega = 0$ can be easily derived from this Wigner function as follows:

$$\begin{aligned} &|\psi(x_1,x_2)|^2\\ &\quad = \int W_{D_1,D_2}(x_1,y_1;x_2,y_2)dy_1dy_2\\ &\quad = (2/\sqrt{\pi})\mathrm{e}^{-r}\exp[-(x_1+x_2)^2\mathrm{e}^{-2r} - (x_1-x_2)^2\mathrm{e}^{2r}]\,,\\ &\qquad \to C'\delta(x_1-x_2) \quad \text{as} \quad r\to\infty\,, \end{aligned} \tag{39a}$$

or alternatively,

$$|\varphi(y_1, y_2)|^2 = \int W_{D_1,D_2}(x_1, y_1; x_2, y_2)dx_1 dx_2$$
$$= (2/\sqrt{\pi})e^{-r} \exp[-(y_1 - y_2)^2 e^{-2r} - (y_1 + y_2)^2 e^{2r}],$$
$$\to C'\delta(y_1 + y_2) \quad \text{as} \quad r \to \infty. \tag{39b}$$

Here the constants C and C' are the normalization constants for the Wigner function and wavefunction, respectively.

As is well-known in the quantum theory of light, each mode of the light field is analogous to a (mechanical) harmonic oscillator, where the position x and momentum p of the oscillator are associated with quadrature-phase amplitudes X and Y of the field mode, as can be justified by the commutation relation $[X, Y] = 2i$. Therefore, in the limiting case of $r \to \infty$, both the Wigner function in (38) and the wavefunctions in (39a, b) for the system of the NOPA have a one-to-one correspondence with the Wigner function and wave functions in the original gedanken experiment of EPR [36].

Since the limiting case $r \to \infty$ corresponds to the situation of infinite gain, it is clear that in order to demonstrate experimentally the EPR paradox for the system of the NOPA, we need to formulate a somewhat different approach than that given above. We will proceed along the lines suggested by Reid [21]. First of all, recall that for the system discussed by EPR [22], two spatially separated particles have their positions and momenta correlated with each other so that "without disturbance" of particle 1, a measurement of the position x_2 of particle 2 can be used to infer (with probability 1) a value for the position x_1 of particle 1 and likewise for the momenta. Thus with their definition of physical reality, EPR claimed that the position and momentum of particle 1 are realistic physical quantities independent of any observers and have definite prescribed values. But this obviously is in contradiction with the Heisenberg uncertainty principle; hence a paradox arises. In a practical system such as the NOPA, however, the parametric gain is of course finite and losses are also present resulting in imperfect correlations between the signal and idler beams. As well our measurements of the quadrature-phase amplitudes are not perfect. Thus the inferences at a distance cannot be made with probability 1 but only with some nonzero errors specified by $\Delta_{\text{inf}}X$ and $\Delta_{\text{inf}}Y$ for X_1 and Y_1, respectively. Fortunately, this non-ideal circumstance does not prevent us from demonstrating the EPR paradox because the paradox is ultimately about the quantitative precision of inference for the quadrature-phase amplitudes of the signal beam (X_1, Y_1) from measurements on those of the spatially separated idler beam (X_2, Y_2). This inference need only be such that the product of uncertainties is below the (apparent) bound set by the uncertainty principle. Hence we can still proceed with a modified form of EPR's argument as follows [21]. A spatially separated measurement of X_2 will specify a value for X_1 not with probability 1 but with average error $\Delta_{\text{inf}}X$; therefore we can establish a value for X_1 to within an error $\Delta_{\text{inf}}X$. Similarly, Y_1 can be determined to within an error $\Delta_{\text{inf}}Y$. From quantum theory, X_1 and Y_1 are noncommuting canonical observables and their variances should satisfy the Heisenberg uncertainty relation $\Delta X_1^2 \Delta Y_1^2 \geq 1$. A paradox in the sense of EPR exists if we can determine the inference errors $\Delta_{\text{inf}}X$ and $\Delta_{\text{inf}}Y$ so that $\Delta_{\text{inf}}X \Delta_{\text{inf}}Y < 1$. For our particular case, the error $\Delta_{\text{inf}}X$ in the inference of X_1 from a measurement of X_2 is given by the variance $V_- = \langle (X_1 - X_2)^2 \rangle$ and similarly for $Y_{1,2}$ with $V_+ = \langle (Y_1 + Y_2)^2 \rangle$. However, as was discussed in (25, 26) of Sect. 1, the quantities $(\lambda X_2, -\lambda Y_2)$ are better estimators of (X_1, Y_1) since $V_\pm^\lambda \leq V_\pm$ because of the limited (non-ideal) degree of correlation.

If we limit our discussion to the system of NOPA with vacuum input, the whole argument given in the previous paragraph can be equivalently formulated in terms of conditional variances [39]. To see this, note that the output fields of the NOPA are described by a Gaussian distribution (38); therefore the variance of X_1 given the value of X_2 or the conditional variance $V(X_1 \mid X_2)$ can be written as (Eq. (9) of [39])

$$V(X_1 \mid X_2) = V_{X_1}(1 - C_{X_1X_2}^2)$$
$$= V_{X_1} - \langle X_1 X_2 \rangle^2 / V_{X_2}, \tag{40}$$

where $C_{X_1X_2}^2 \equiv |\langle X_1 X_2 \rangle - \langle X_1 \rangle \langle X_2 \rangle|^2 / V_{X_1} V_{X_2}$ and we have used the fact that $\langle X_1 \rangle = \langle X_2 \rangle = 0$ ($V_{X_1} \equiv \langle \Delta X_1^2 \rangle$, $V_{X_2} \equiv \langle \Delta X_2^2 \rangle$ are the ordinary unconditional variances). But from (4.4) of [21] the rhs of (40) is just $V_-^\lambda \equiv \langle (X_1 - \lambda X_2)^2 \rangle$ with λ optimized. Hence

$$V(X_1 \mid X_2) = V_-^\lambda, \tag{41a}$$

and likewise

$$V(Y_1 \mid Y_2) = V_+^\lambda. \tag{41b}$$

Thus with the conditional variances $V(X_1 \mid X_2)$, $V(Y_1 \mid Y_2)$, we can arrive at the same results as we did with the inference errors $\Delta_{\text{inf}}X$ and $\Delta_{\text{inf}}Y$. Only this time, the discussion leading to the paradox is more direct because in EPR's original argument, the existence of the realistic object X_1 is determined from the measured value of X_2 in the sense of a conditional distribution. We should note that in quantum mechanics there is in fact no conflict between the inequalities $\Delta X_1^2 \Delta Y_1^2 \geq 1$ and $V(X_1 \mid X_2) V(Y_1 \mid Y_2) = \Delta_{\text{inf}}^2 X \Delta_{\text{inf}}^2 Y < 1$ since the first inequality refers to unconditional and independent measurements of X_1 and Y_1, while the second inequality refers to the conditional measurement of X_1 given X_2 and likewise for $(Y_1, -Y_2)$. The absence of an unresolvable paradox for our system as well as for the historical system of EPR will be discussed more fully in Sect. 4.

In our experiment, the quadrature-phase amplitudes $X_1(\phi_1)$ and $X_2(\phi_2)$ of the signal and idler beams are measured with two homodyne detection schemes (Sect. 3 and Fig. 3b). The photocurrent $i_2(t)$ associated with the idler beam is attenuated by a factor λ and then subtracted from the photocurrent $i_1(t)$ associated with the signal beam. The combined photocurrent $i_-(t) = i_1(t) - \lambda i_2(t)$, which reflects the fluctuations of the quantity $X_1(t, \phi_1) - \lambda X_2(t, \phi_2)$, is then sent to a spectral analyzer (SA). The spectral analyzer gives the power spectrum $\Phi(\Omega, \phi_1, \phi_2)$ for the current $i_-(t)$ at a particular analysis frequency Ω; this spectrum is proportional to the quantities $V_{12}^\lambda(\Omega, \phi_1, \phi_2)$ calculated in the preceding section. By using the shot noise level Ψ_{0s} as ref-

erence (where Ψ_{0s} is the spectral density for a vacuum-state signal beam at the balanced detector H1 with $\lambda = 0$), we can measure $V_{12}^{\lambda}(\Omega, \phi_1, \phi_2) = \Phi(\Omega, \phi_1, \phi_2)/\Psi_{0s}$ and make a comparison with the result in (29c). As for the measurement of the inference errors $\Delta_{\text{inf}}X$, $\Delta_{\text{inf}}Y$, and the EPR paradox, we will see in the following discussion how the EPR paradox can be formulated in terms of the spectral densities $V_{12}^{\lambda}(\Omega, \phi_1, \phi_2)$, where now we are dealing with the spectral components $X_{1,2}(\Omega)$ and $Y_{1,2}(\Omega)$ defined in (14). Notice that in the experiment, we measure the inference errors $\Delta_{\text{inf}}X$, $\Delta_{\text{inf}}Y$ but not the conditional variances $V(X_1 \mid X_2)$ and $V(Y_1 \mid Y_2)$, although they should be the same for our system (41).

From (25), it is clear that $V_{\pm}^{\lambda}(\Omega)$ are associated with the degree of correlation of the quantities $X_{1,2}(\Omega)$, $Y_{1,2}(\Omega)$ and hence with the error of inference in determining $[X_1(\Omega), Y_1(\Omega)]$ from $[X_2(\Omega), -Y_2(\Omega)]$. However, $X_{1,2}(\Omega)$ and $Y_{1,2}(\Omega)$ are not Hermitian operators and therefore are not directly observable. Consider instead the following two pairs of Hermitian observables for the NOPA system [21]:

$$\begin{aligned} \text{Re}^* X_{1,2}(\Omega) &\equiv [X_{1,2}(\Omega) + X_{1,2}^{\dagger}(\Omega)]/\sqrt{2}\,, \\ \text{Re}^* Y_{1,2}(\Omega) &\equiv [Y_{1,2}(\Omega) + Y_{1,2}^{\dagger}(\Omega)]/\sqrt{2}\,, \end{aligned} \tag{42a}$$

and the corresponding imaginary parts,

$$\begin{aligned} \text{Im}^* X_{1,2}(\Omega) &\equiv [X_{1,2}(\Omega) - X_{1,2}^{\dagger}(\Omega)]/\sqrt{2}\text{i}\,, \\ \text{Im}^* Y_{1,2}(\Omega) &\equiv [Y_{1,2}(\Omega) - Y_{1,2}^{\dagger}(\Omega)]/\sqrt{2}\text{i}\,, \end{aligned} \tag{42b}$$

with $X_{1,2}(\Omega)$ and $Y_{1,2}(\Omega)$ given in (14). Obviously $\text{Re}^* X_{1,2}(\Omega) = \text{Re}^* X_{1,2}(-\Omega)$, etc., so that we can limit our discussion to $\Omega > 0$. With the commutation relations $[D_{1,2}(\Omega), D_{1,2}^{\dagger}(\Omega')] = \delta(\Omega - \Omega')$, we can easily prove from (14, 42) that

$$[\text{Re}^* X_{1,2}(\Omega), \text{Re}^* Y_{1,2}(\Omega')] = 2\text{i}\delta(\Omega - \Omega')\,,$$

$$[\text{Im}^* X_{1,2}(\Omega), \text{Im}^* Y_{1,2}(\Omega')] = 2\text{i}\delta(\Omega - \Omega')\,,$$

with all other commutators equal to zero. The Heisenberg uncertainty relations for the observables $\text{Re}^* X_{1,2}$, etc. can then be formulated as follows

$$\left.\begin{aligned} S_{1,2}^{\text{Re}\,X}(\Omega) S_{1,2}^{\text{Re}\,Y}(\Omega) &\geq 1\,, \\ S_{1,2}^{\text{Im}\,X}(\Omega) S_{1,2}^{\text{Im}\,Y}(\Omega) &\geq 1\,, \end{aligned}\right\} \tag{43a}$$

where for stationary processes, the spectra $S_{1,2}^{\text{Re}\,X}(\Omega)$, etc. are defined by

$$\langle \text{Re}^* X_{1,2}(\Omega) \text{Re}^* X_{1,2}(\Omega') \rangle \equiv S_{1,2}^{\text{Re}\,X}(\Omega)\delta(\Omega - \Omega') \tag{44}$$

and similarly for the other quantities. From (44), it is obvious that $S_{1,2}^{\text{Re}\,X}(\Omega)$, etc. characterize the fluctuations of $\text{Re}^* X_{1,2}(\Omega)$, etc. and are associated with the variances $\Delta^2 \text{Re}^* X_{1,2}(\Omega) \equiv S_{1,2}^{\text{Re}\,X}(\Omega)$, etc. for $\text{Re}^* X_{1,2}(\Omega)$, etc. The Heisenberg uncertainty relation for $\text{Re}^* X_{1,2}(\Omega)$, $\text{Re}^* Y_{1,2}(\Omega)$ can be written as

$$\Delta^2 \text{Re}^* X_{1,2}(\Omega) \Delta^2 \text{Re}^* Y_{1,2}(\Omega) \geq 1\,. \tag{43b}$$

Let us now form the correlation quantities

$$\begin{aligned} \text{Re}\,\Delta_-(\Omega) &= \text{Re}^* X_1(\Omega) - \lambda \text{Re}^* X_2(\Omega)\,, \\ \text{Re}\,\Delta_+(\Omega) &= \text{Re}^* Y_1(\Omega) + \lambda \text{Re}^* Y_2(\Omega)\,, \\ \text{Im}\,\Delta_-(\Omega) &= \text{Im}^* X_1(\Omega) - \lambda \text{Im}^* X_2(\Omega)\,, \\ \text{Im}\,\Delta_+(\Omega) &= \text{Im}^* Y_1(\Omega) + \lambda \text{Im}^* Y_2(\Omega)\,, \end{aligned} \tag{45}$$

where we have for their spectra (as in (44)),

$$\begin{aligned} \langle \text{Re}\,\Delta_{\pm}(\Omega) \text{Re}\,\Delta_{\pm}(\Omega') \rangle &\equiv V_{\pm}^{\text{Re}}(\Omega)\delta(\Omega - \Omega')\,, \\ \langle \text{Im}\,\Delta_{\pm}(\Omega) \text{Im}\,\Delta_{\pm}(\Omega') \rangle &\equiv V_{\pm}^{\text{Im}}(\Omega)\delta(\Omega - \Omega')\,, \end{aligned} \tag{46}$$

With the above equations, we can rewrite the left-hand-side of (25) as

$$\begin{aligned} &\langle [X_1(\Omega) - \lambda X_2(\Omega)] [X_1(\Omega') - \lambda X_2(\Omega')] \rangle \\ &\quad \equiv \Delta_{\text{inf}}^2 X(\Omega)\delta(\Omega + \Omega') \\ &\quad = \langle [X_1(\Omega) - \lambda X_2(\Omega)] [X_1^{\dagger}(-\Omega') - \lambda X_2^{\dagger}(-\Omega')] \rangle \\ &\quad = \frac{1}{2} \langle [\text{Re}\,\Delta_-(\Omega) + \text{i}\,\text{Im}\,\Delta_-(\Omega)] \\ &\qquad \times [\text{Re}\,\Delta_-(-\Omega') - \text{i}\,\text{Im}\,\Delta_-(-\Omega')] \rangle \\ &\quad = \frac{1}{2} [V_-^{\text{Re}}(\Omega) + V_-^{\text{Im}}(\Omega)]\delta(\Omega + \Omega') \\ &\quad = V_-^{\text{Re}}(\Omega)\delta(\Omega + \Omega')\,, \end{aligned} \tag{47}$$

where the final step follows since $V_{\pm}^{\text{Re}}(\Omega) = V_{\pm}^{\text{Im}}(\Omega)$ for stationary processes. Comparing (25) and (47), we have

$$V_-^{\text{Re}}(\Omega) = V_-^{\text{Im}}(\Omega) = V_-^{\lambda}(\Omega) = \Delta_{\text{inf}}^2 X(\Omega)\,. \tag{48a}$$

Similarly

$$V_+^{\text{Re}}(\Omega) = V_+^{\text{Im}}(\Omega) = V_+^{\lambda}(\Omega) = \Delta_{\text{inf}}^2 Y(\Omega)\,. \tag{48b}$$

Therefore, in the inference of $\text{Re}^* X_1(\Omega)\,[\text{Re}^* Y_1(\Omega)]$ from $\lambda \text{Re}^* X_2(\Omega)\,[-\lambda \text{Re}^* Y_2(\Omega)]$, the inference error is $V_-^{\text{Re}}(\Omega) = \Delta_{\text{inf}}^2 X(\Omega)[V_+^{\text{Re}}(\Omega) = \Delta_{\text{inf}}^2 Y(\Omega)]$ because of (48a) [(48b)]. Thus there exists an EPR paradox if

$$V_-^{\text{Re}}(\Omega) V_+^{\text{Re}}(\Omega) < 1 \tag{49a}$$

or

$$\Delta_{\text{inf}}^2 X(\Omega) \Delta_{\text{inf}}^2 Y(\Omega) < 1 \tag{49b}$$

in apparent contradiction with the uncertainty relations in (43a, b). A similar discussion can be applied to $\text{Im}^* X_{1,2}(\Omega)$ and $\text{Im}^* Y_{1,2}(\Omega)$. Note that $V_{\pm}^{\lambda}(\Omega)$ are strictly associated with $X_{1,2}(\Omega) = (\text{Re}^* X_{1,2} + \text{i}\,\text{Im}^* X_{1,2})/\sqrt{2}$ and $Y_{1,2}(\Omega) = (\text{Re}^* Y_{1,2} + \text{i}\,\text{Im}^* Y_{1,2})/\sqrt{2}$ so that our measurements of $V_{\pm}^{\lambda}(\Omega)$ (without coherent detection of the individual quadratures at Ω) are actually measurements of $V_{\pm}^{\text{Re}}(\Omega) + V_{\pm}^{\text{Im}}(\Omega)$ rather than $V_{\pm}^{\text{Re}}(\Omega)$ or $V_{\pm}^{\text{Im}}(\Omega)$ alone. But with the reasonable assumption of stationarity, the results of (48, 49) follow. Thus the measurement of $V_{\pm}^{\lambda}(\Omega)$ [and hence of $\Delta_{\text{inf}}^2 X(\Omega)$ and $\Delta_{\text{inf}}^2 Y(\Omega)$] is sufficient to give $V_{\pm}^{\text{Re}}(\Omega)$ or $V_{\pm}^{\text{Im}}(\Omega)$ and to demonstrate the EPR paradox if the condition in (49a, b) can be achieved [21].

3 Experimental Configuration

For our experiment, we have constructed a nondegenerate optical parametric oscillator with the signal (mode 1) and idler (mode 2) beams generated as the output modes ($b_1^{(o)}$, $b_2^{(o)}$) shown in Fig. 2. The pump strength is controlled such that the oscillator is always operated below threshold. As discussed in Sect. 1, such a device can be viewed as a nondegenerate optical parametric amplifier (NOPA) with the

gain determined by the pump strength and with a bandwidth limited by the cavity linewidth (which is typically much smaller than the phase matching bandwidth of the nonlinear medium). Nondegeneracy is realized in our work via a Type II parametric process where the two down-converted modes (signal and idler) have orthogonal polarization. A more detailed diagram of the experimental arrangement is shown in Fig. 3. The NOPA consists of a folded ring cavity of total length 38 cm with two curved mirrors (M3, M4) of 10 cm radius of curvature and two flat mirrors (M1, M2). Three of the mirrors (M2, M3, M4) have high reflectivity (99.98%) at 1.08 μm and relatively high transmission (94–96%) at 0.54 μm. M1 is the output coupler for the subharmonic field at 1.08 μm with a transmission coefficient of 3%. The nonlinear medium is placed between the two curved mirrors where the small waist of the cavity is located (approximate waist size $\omega_0 = 60\,\mu\text{m}$).

The crystal for the down-conversion process is a $3 \times 3 \times 10\,\text{mm}^3$, a-cut potassium titanyl phosphate (KTP) crystal with two faces dual-band antireflection coated to minimize the loss at 1.08 μm and 0.54 μm. The two modes (signal and idler) are polarized along the b and c axes of the crystal, respectively. Type II *noncritical* phase matching at 1.08 μm is achieved at a temperature of 63° C with a full width of about 30° C [40, 41]. Because of the nature of Type II processes, both the b- and c-polarized beams are not usually simultaneously resonant for a given cavity length. However, the b- and c-polarized beams have different temperature dependences for their indices of refraction inside the crystal, so that by fine tuning of the crystal temperature, we can reach the condition of simultaneous resonance for the signal and idler fields (a_1, a_2). For our arrangement, the temperature tolerance to maintain the dual resonance condition is about 20 mK and the separation between two consecutive overlapping resonances of the b- and c-polarized beams is about 10° C. An active stabilization circuit is used in order to fix the crystal temperature to a few mK.

We employ the well-known Pound-Drever rf sideband technique [42] to lock the NOPA cavity onto resonance for the signal mode (b-polarization) with the help of an auxiliary beam that is counter-propagating relative to the down-converted beams (modes 1, 2) from the pump field (beam ε_1 and detector D2 in Fig. 3a). Such a beam does not adversely affect the system performance as long as the backscattering is small (in our case $< 10^{-4}$). Once the signal mode (a_1) is locked on resonance, an adjustment of the temperature of the crystal brings the orthogonal idler mode (a_2) into resonance.

The NOPA cavity is pumped at 0.54 μm with a beam polarized along the b-axis that is coupled into the cavity through mirror M4, which has a transmission coefficient of 96% at 0.54 μm. The green pump power is built up in an independent cavity formed by the high reflector mirrors M5 through M8 and the input coupler W (a window with an antireflection coating on one side). The green build-up cavity is also locked on resonance with the Pound-Drever technique by detector D3. Due to the reflection losses of the mirrors M3 and M4 at 0.54 μm, this cavity has a modest build up of about 5 times. We have chosen this design of two independent cavities for 1.08 μm and 0.54 μm to avoid the technical problems that we have previously encountered in triply resonant cavities [4]. The injected green pump power before

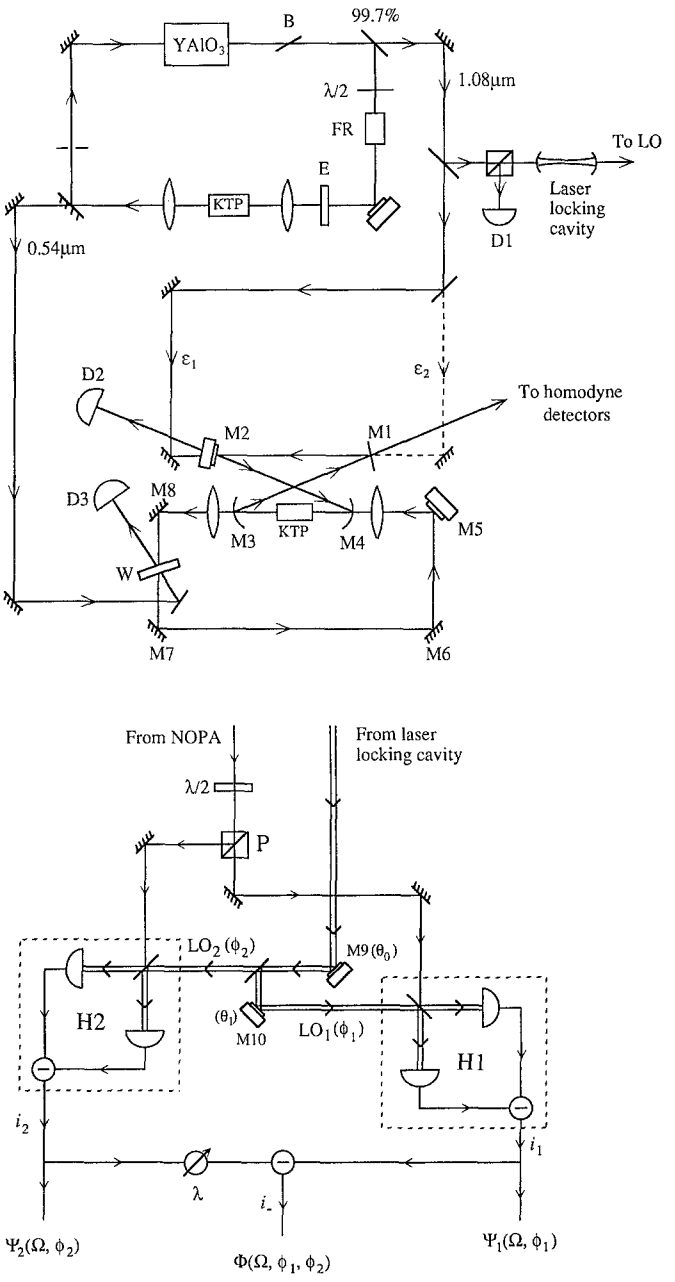

Fig. 3. a Experimental schematic of the NOPA and the laser system. **b** Diagram of the dual balanced homodyne detectors (H_1, H_2), showing the photocurrents i_1, i_2 and i_- that correspond to $\Psi_1(\Omega, \phi_1)$, $\Psi_2(\Omega, \phi_2)$ and $\Phi(\Omega, \phi_1, \phi_2)$

build-up can be varied from 10 mW up to about 90 mW. The injected green power for the threshold of the NOPA is approximately $P_{\text{th}} = 150\,\text{mW}$.

The field at 0.54 μm is itself generated by intracavity harmonic conversion in a frequency stabilized, TEM_{00} Nd : $YAlO_3$ laser. As shown in Fig. 3a, the laser is a ring cavity containing an a-cut $2 \times 2 \times 6.8\,\text{mm}^3$ KTP crystal located between two lenses with 5 cm focal length for intracavity frequency doubling. The laser frequency is locked to an external cavity with the Pound-Drever sideband technique by detector D1 and its rms linewidth is approximately 50 kHz. The fundamental beam at 1.08 μm transmitted through the laser locking cavity (which also acts as a filter cavity for the

spatial mode of the beam) is intensity-stabilized and then split into two beams to serve as local oscillators for the balanced homodyne detectors (H1, H2). Fractions of the fundamental beam are used to lock the NOPA cavity (ε_1) with an error signal derived at detector D2 and to provide a probe beam (ε_2) for the NOPA.

To quantify the operating parameters for the NOPA, we inject an intense probe beam (ε_2) at the fundamental frequency into the cavity via the input coupler M1 with the cavity used as a frequency doubler without green pump. In this way, we can make quantitative measurements of the conversion efficiency of the crystal and the linear losses of the cavity [41]. The generated green light also helps us to align the green build-up cavity and to mode-match it to the NOPA cavity. We then measure the classical gain of the amplifier by turning on the green pump and injecting a weak probe beam ε_2 with various polarizations through the input coupler M1. When the injected beam has the same polarization as either the signal or idler beams, we observe phase-insensitive gain for the beam through mirror M2. When the injected beam is polarized at $\pm 45°$ relative to the b-axis, we observe phase-sensitive gain that is the same for both $\pm 45°$ polarizations. By way of these tests, we have concluded that our system behaves as an NOPA with two independent signal and idler modes (b and c axes).

Beyond the generation scheme, a detailed diagram of the detection system is drawn in Fig. 3b. The output beams from the NOPA are separated with a low loss polarization beamsplitter (P). Each beam is then combined with a local oscillator by a 50:50 beam splitter to form a balanced homodyne detection scheme [43]. We denote LO_1 and LO_2 as the local oscillators corresponding to the homodyne detection schemes (H1, H2). The photocurrents $i_1(t)$, $i_2(t)$ from (H1, H2) are sent either directly to a spectrum analyzer for measurements of their spectral densities or to a hybrid junction with a phase shift of 180°, where $i_2(t)$ passes first through an attenuator λ. The spectral density of the combined current $i_-(t) = i_1(t) - \lambda i_2(t)$ can then also be measured.

The spectral densities of the photocurrents $i_1(t)$, $i_2(t)$, and $i_-(t)$ recorded by the spectrum analyzer are given by

$$\begin{aligned}
\Psi_1(\Omega) &= \int \langle \Delta i_1(t) \Delta i_1(t+\tau) \rangle e^{i\Omega\tau} d\tau \,, \\
\Psi_2(\Omega) &= \int \langle \Delta i_2(t) \Delta i_2(t+\tau) \rangle e^{i\Omega\tau} d\tau \,, \\
\Phi(\Omega) &= \int \langle \Delta i_-(t) \Delta i_-(t+\tau) \rangle e^{i\Omega\tau} d\tau \,,
\end{aligned} \tag{50}$$

where Ω is the analysis frequency of the spectral analyzer; $\Omega/2\pi = 1.1\,\mathrm{MHz}$ for all data reported here. If we denote ϕ_1 as the phase difference between LO_1 and the signal beam, and ϕ_2 as the phase difference between LO_2 and the idler beams, then the photocurrents i_1, i_2 reflect the fluctuations of the quadrature-phase amplitudes (as in (28))

$$\begin{aligned}
Z_1(t, \phi_1) &\equiv O_1(t) e^{-i\phi_1} + O_1^\dagger(t) e^{i\phi_1} \,, \\
Z_2(t, \phi_2) &\equiv O_2(t) e^{-i\phi_2} + O_2^\dagger(t) e^{i\phi_2} \,,
\end{aligned}$$

where $O_{1,2} = (D_{1,2}^{(o)}$ or $\bar{D}_{1,2}^{(o)})$ and $Z_{1,2} = (X_{1,2}$ or $\bar{X}_{1,2})$. Thus, depending on the arrangement of the half waveplate which directs the fields to H1, H2 and upon the phase settings of the fields, we can measure the vaious noise spectra that were derived in Sect. 1.

The local oscillator beam originates from the laser at the fundamental frequency. It passes through a spatial mode cleaning cavity (which also serves as the laser locking cavity) and then is divided into LO_1 and LO_2 by a 50:50 beam splitter. The phases ϕ_1, ϕ_2 of the local oscillators LO_1 and LO_2 can be varied by scanning the steering mirrors M9 (θ_0), M10 (θ_1), which are mounted on piezoelectric transducers. The intensities of the local oscillators are actively stabilized (to about 1%) with a servo based upon a combination of an electrooptic modulator and a polarizer.

We have used a procedure similar to that described in [1b] to test our homodyne detection scheme. The balancing and calibration of the homodyne detectors are done by fine adjustment of the electronic gains and relative phases of the detectors through their shot-noise levels and with external coherent amplitude modulation. The excess amplitude noise of the two local oscillator beams above the shot-noise level is measured to be less than 0.2 dB and is suppressed in the balanced homodyne detection schemes by about 30 dB. Overall, the shot-noise level at the analyzing frequency is determined to within ± 0.1 dB and is principally limited by small drifts of the radio frequency Ω, which have a disproportionate effect due to the resonant nature of the detection electronics. Our detectors give a shot-noise level 25 dB above the electronic noise floor for a local oscillator power of 1 mW [44].

3.1 Measurements of Squeezing

To investigate the quantum noise of the system, we start by measuring the spectra of squeezing for the modes $\bar{D}_{1,2}^{(o)}$ by projecting the signal and idler fields along polarization directions at $\pm 45°$ relative to the signal polarization [2]. This is easily done by changing the setting of the half waveplate ($\lambda/2$) placed at the NOPA output. Individual spectra of squeezing can then be determined with the two balanced detectors (H1, H2) from the spectral densities $\Psi_{1,2}$ of photocurrent fluctuations for $i_{1,2}$. By scanning the overall local oscillator phase θ_0, we observe noise variations above and below the vacuum-state levels from which $\Psi_-(\Omega)$ (maximum noise reduction) and $\Psi_+(\Omega)$ (maximum noise enhancement) can be determined. Figure 4 shows a trace for the squeezing at detector H1, where the shot-noise level is denoted by Ψ_{01}. $\Psi_-(\Omega)$ and $\Psi_+(\Omega)$ are measured from a number of traces as in Fig. 4 for five different green pump powers of the NOPA over a range from 10 to 90 mW and are used to derive the overall loss as well as the quantum noise gain of the system. By considering that this system should produce a minimum uncertainty state under the condition of no loss [1, 37], we are able to determine that the overall loss is 0.37. This result is comparable to the measured overall loss of $L_{\mathrm{overall}} = 0.31$ derived from measurements of the individual losses for the system. From (31) we have

$$L_{\mathrm{overall}} = 1 - \frac{\gamma}{\varrho + \gamma} T_0 \eta^2 \alpha \,; \tag{51}$$

where $(1 - L) \equiv T_0 \eta^2 \alpha$, with the individual efficiencies given as follows.

– Cavity escape efficiency $\gamma/(\varrho + \gamma) = 90\%$ (we suspect that the uncertainty in the measurement of this quantity con-

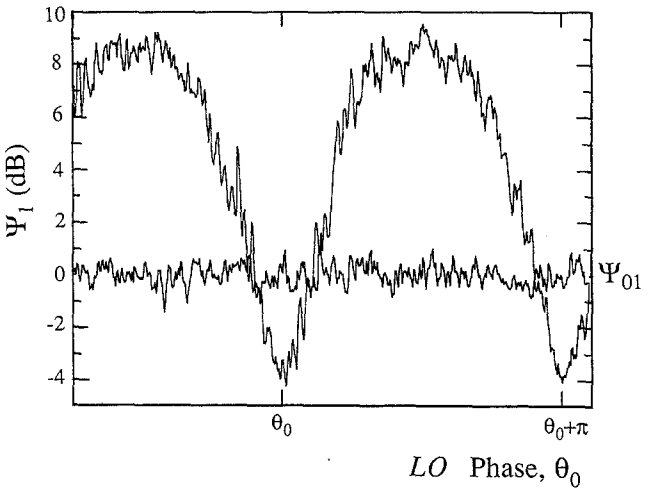

Fig. 4. Phase dependence of the quantum noise Ψ_1 in a squeezed state produced from the projection of the signal and idler fields from the NOPA along a direction at 45° relative to the signal beam polarization. Ψ_{01} is the vacuum-state noise level. Analysis frequency $\Omega/2\pi$ = 1.1 MHz, resolution bandwidth=100 kHz, video bandwidth=2.2 kHz, scan time=100 ms

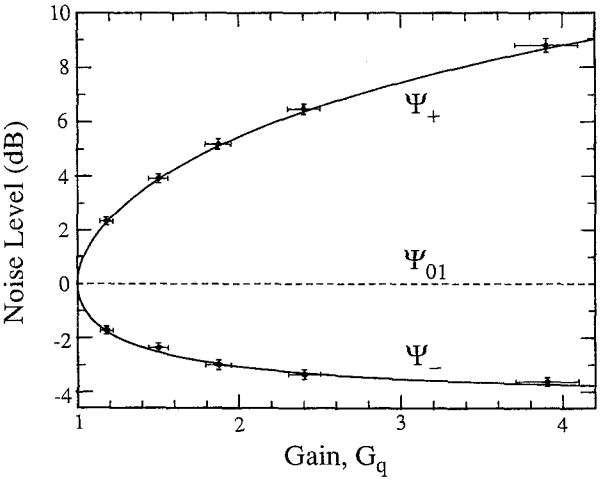

Fig. 5. Logarithm of the observed noise levels Ψ_+ (maximum) and Ψ_- (minimum) versus the quantum noise gain G_q for a squeezed beam from the NOPA. Analyzer settings are the same as in Fig. 4, and Ψ_{01} is the vacuum-noise level. The theoretical fit shown as a solid line is derived from (32), with $L_{\text{overall}} = 0.37$

tributes to most of the discrepancy between the derived and directly measured overall losses);
- Propagation efficiency T_0 (mainly from the polarizer P) = 95%;
- Homodyne efficiency $\eta = 95\%$ for H1 and 96% for H2;
- Detector quantum efficiency $\alpha = 90\%$ for H1 and 80% for H2.

In Fig. 5, we show the measured maximum Ψ_+ and minimum Ψ_- noise levels vs the quantum noise gain G_q for five different pump powers of the NOPA. The quantum noise gain $G_q(\Omega)$ is derived from $\Psi_\pm(\Omega)$ with the following definition:

$$G_q(\Omega) = [\Psi_-(\Omega) + \Psi_+(\Omega)]/2\Psi_{01}(\Omega), \quad (52)$$

where we have used (27a–c) with $S_\pm = \Psi_\pm/\Psi_{01}$. The solid curves are drawn according to (32a–d) in Sect. 1, where the overall loss L_{overall} is chosen to be 0.37 and the normalized analysis frequency ω is derived to be 0.56 from (33) with measured finesse $F_m = 180$, analysis frequency $\Omega/2\pi$ = 1.1 MHz and cavity free spectral range $\nu_{FSR} = 790$ MHz. The relatively good agreement between the measured and calculated spectra establishes some confidence in the performance of our system as a simple NOPA describable by the theory of Sect. 1 and provides as well the number of 37% for the overall loss of the system.

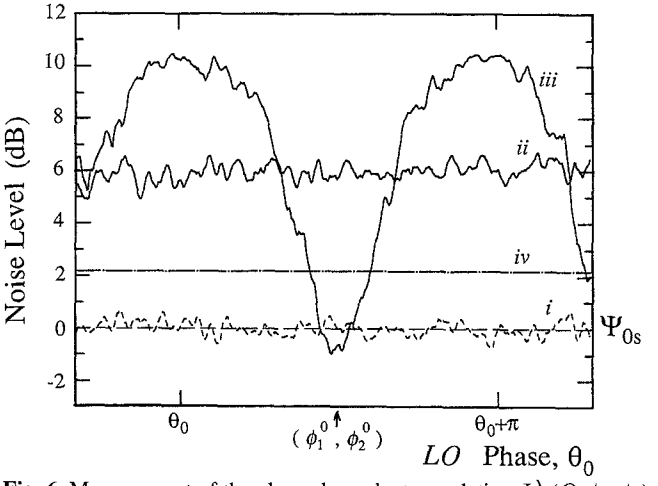

Fig. 6. Measurement of the phase-dependent correlation $\Phi_{12}^\lambda(\Omega, \phi_1, \phi_2)$ between the signal and idler beams from the NOPA as a function of overall LO phase θ_0, where (i) represents the shot-noise level of signal beam alone (Ψ_{0s}); (ii) is the phase-insensitive noise of signal beam from the NOPA (G_q); (iii) is the phase sensitive noise $\Phi_{12}^\lambda(\Omega, \phi_1, \phi_2)$ with the attenuation factor $\lambda = 0.78$; (iv) is the shot-noise level for the photocurrent $i_- = i_1 - \lambda i_2$ (corresponding to $X_1 - \lambda X_2$). Acquisition parameters are the same as in Fig. 4 with a smoothing algorithm applied to the traces for clarification

3.2 Measurements of EPR Correlations

Having investigated squeezed state generation in the ±45° modes, we next project back the original directions of polarizations for the signal and idler fields with an adjustment of the half waveplate after the NOPA. The signal and idler beams are then directed to the two spatially separated homodyne detectors (H1, H2), where the correlations between the quadrature-phase amplitudes of these two beams can be studied by measuring the spectral density $\Phi(\Omega, \phi_1, \phi_2)$ for the current $i_-(t)$ (Fig. 3b).

As illustrated in Fig. 6, a phase-sensitive variation of $\Phi(\Omega, \phi_1, \phi_2)$ is observed as the phase θ_0 is scanned (note that $\phi_1 = \theta_0 + \delta\theta_{01}$ and $\phi_2 = \theta_0 + \delta\theta_{02}$ with $\delta\theta_{01,02}$ as arbitrary offsets). When the phase $\phi_1 + \phi_2 = 2p\pi$ (p =integer), $\Phi(\Omega, \phi_1, \phi_2)$ corresponds to $V_\pm^\lambda(\Omega)$ (29c), where the attenuation factor λ is adjusted to minimize the value of $V_\pm^\lambda(\Omega)$. On the other hand, if $\lambda = 0$ we examine the quadrature-phase amplitudes of the signal beam alone. In this case, we observe large phase-insensitive quantum noise which results from the amplification of the vacuum-noise input to the NOPA. From the level of this noise (relative to the vacuum-noise level),

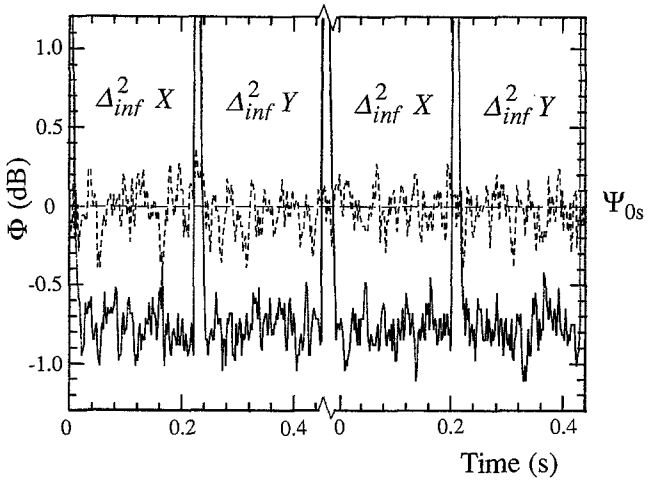

Fig. 7. Spectral density of the photocurrent fluctuations $\Phi^{\lambda}_{12}(\Omega, \phi_1, \phi_2)$ vs time where first the variance $\Delta^2_{\text{inf}}X(\Omega)$ and then the variance $\Delta^2_{\text{inf}}Y(\Omega)$ are measured as the phases θ_0 and θ_1 of the local oscillators LO_1 and LO_2 are stepped according to the discussion in the text. Two separated measurements for the pair $(\Delta^2_{\text{inf}}X, \Delta^2_{\text{inf}}Y)$ are shown. Ψ_{0s} is the vacuum-state level for the signal beam alone. Analysis frequency $\Omega/2\pi = 1.1$ MHz, rf bandwidth=100 kHz, video bandwidth=0.2 kHz

we can find the phase-insensitive quantum noise gain $G_q(\Omega)$. Under the same conditions ($\lambda = 0$), when we block the input to the homodyne detector H1, $\Phi(\Omega, \phi_1, \phi_2) \equiv \Psi_{0s}$ gives the vacuum-noise level of mode 1 (signal) alone, which corresponds to unity in the right-hand-side of the inequalities (43, 49). A typical set of such measurements is displayed in Fig. 6 for a pump intensity of about 90 mW. Trace (i) is the shot noise level Ψ_{0s} of the signal beam alone; trace (ii) is the amplified phase-insensitive quantum noise of the signal beam (G_q); trace (iii) shows the phase-sensitive quantum noise Φ as θ_0 is scanned, where λ has been optimized to be 0.78; trace (iv) corresponds to the shot-noise level for the combination $X_1 - \lambda X_2$, which is a factor of $1 + \lambda^2$ higher than the level of unity for the shot-noise level of the signal beam alone. From these traces, we see that the noise spectrum of the signal beam alone (ii) is phase-insensitive and has an excess noise about 5.5 dB above the vacuum-state or shot-noise level Ψ_{0s} (i); thus the quantum noise gain G_q is determined to be 3.8. Note that the phase-sensitive noise $\Phi(\Omega, \phi_1, \phi_2)$ (iii) for some value of phases (ϕ^0_1, ϕ^0_2) is below both the shot-noise levels of the signal beam alone (i) and of the combination $X_1 - \lambda X_2$ (iv) by about 0.8 dB and 3 dB, respectively. This means a demonstration of the EPR paradox is possible (as determined by the level of trace (i)) and the Cauchy-Schwartz inequality for classical wave theory is violated (as determined by the level of trace (iv)).

To quantify more carefully the deviations of $\Phi(\Omega, \phi^0_1, \phi^0_2)$ below the vacuum-state level Ψ_{0s} of the signal beam alone and thus to demonstrate the EPR paradox, we stop the scan of θ_0 and manually tune θ_0 to a minimum value of $\Phi(\Omega, \phi_1, \phi_2)$ with corresponding phases (ϕ^0_1, ϕ^0_2) (again with λ chosen at its optimum value). This minimum value of $\Phi(\Omega)$ as compared to the shot-noise level Ψ_{0s} of the signal beam alone gives the quantity $V^{\lambda}_{-}(\Omega)$ [or equivalently $V^{\text{Re}}_{-}(\Omega)$ and $V^{\text{Im}}_{-}(\Omega)$ from (48a) (see the discussion in Sect. 2)]. Hence the inference error $\Delta^2_{\text{inf}}X(\Omega) \sim \langle (X_1 - \lambda X_2)^2 \rangle$ is determined experimentally to be $\Delta^2_{\text{inf}}X(\Omega) = \Phi(\Omega, \phi^0_1, \phi^0_2)/\Psi_{0s}$, where we have arbitrarily chosen $X_1(\phi^0_1)$ as X_1 and $X_2(\phi^0_2)$ as X_2. After recording $\Phi(\Omega, \phi^0_1, \phi^0_2)$ for a period of about 200 ms, we then switch the phases θ_0 and θ_1 shown in Fig. 3b so that $\theta_0 \to \theta_0 + 90°$, $\theta_1 \to \theta_1 + 180°$. This results in $\phi^0_1 \to \phi^0_1 + 270°$, $\phi^0_2 \to \phi^0_2 + 90°$ and therefore $X_1(\phi^0_1) \to X_1(\phi^0_1 + 270°) \equiv -Y_1$ and $X_2(\phi^0_2) \to X_2(\phi^0_2 + 90°) \equiv Y_2$, where $Y_{1,2}$ are the conjugate quadratures of $X_{1,2}$. Hence the conjugate inference error $\Delta^2_{\text{inf}}Y(\Omega) \sim \langle (Y_1 + \lambda Y_2)^2 \rangle$ is determined experimentally to be $\Phi(\Omega, \phi^0_1 + 270°, \phi^0_2 + 90°)/\Psi_{0s}$. Since $\Phi(\Omega, \phi_1, \phi_2)$ depends only on $\cos(\phi_1 + \phi_2)$ (29c), the change $\phi^0_1 + \phi^0_2 \to \phi^0_1 + \phi^0_2 + 360°$ should not alter the value of $\Phi(\Omega, \phi^0_1, \phi^0_2)$. In Fig. 7, we show that this is indeed approximately the case; the solid line in the figure shows two separate measurements of the pair $\Delta^2_{\text{inf}}X(\Omega)$, $\Delta^2_{\text{inf}}Y(\Omega)$ (with about 30 s between them). Note that the phase steps in θ_0, θ_1 are calibrated independently with an interferometer to within 4°. The large increases in Φ located at successive phase steps are because the transition $\phi_1 + \phi_2 \to \phi_1 + \phi_2 + 360°$ passes through the maximum value of $\Phi(\Omega, \phi_1, \phi_2)$ [associated with the fluctuations of e.g., $(X_1 + \lambda X_2)$]. By the technique illustrated in Fig. 7, we first measure the inference error $\Delta^2_{\text{inf}}X(\Omega)$ followed by the (approximately) conjugate inference error $\Delta^2_{\text{inf}}Y(\Omega)$ and hence quantify the errors in determining the conjugate pair (X_1, Y_1) from measurements of the spatially separated quantities $(\lambda X_2, -\lambda Y_2)$.

In order to demonstrate the EPR paradox, we must of course refer our measurements to the value of unity on the right-hand-side of the inequality in (49a, b), which operationally corresponds to the vacuum-noise level Ψ_{0s} of the signal beam (mode 1) alone. This is done by setting λ to zero and blocking all beams from the NOPA. Such measurements are performed both before and after $\Delta^2_{\text{inf}}X(\Omega)$ and $\Delta^2_{\text{inf}}Y(\Omega)$ are recorded, with a typical trace of this shot noise level shown as the dashed curve in Fig. 7. It is clear that both $\Delta^2_{\text{inf}}X(\Omega)$ and $\Delta^2_{\text{inf}}Y(\Omega)$ are smaller than the vacuum-noise level of the signal beam alone. In particular, from this trace we find that relative to Ψ_{0s}, $\Delta^2_{\text{inf}}X(\Omega) = 0.835 \pm 0.008$ [(-0.78 ± 0.04) dB] and $\Delta^2_{\text{inf}}Y(\Omega) = 0.837 \pm 0.008$ [(-0.77 ± 0.04) dB] resulting in a product of inference variances $\Delta^2_{\text{inf}}X(\Omega)\Delta^2_{\text{inf}}Y(\Omega) = (0.70 \pm 0.01) < 1$. This clearly satisfies the inequality in (49a, b) thus providing a realization of the original EPR paradox for continuous variables.

In addition to the quantities $\Delta^2_{\text{inf}}X(\Omega)$, $\Delta^2_{\text{inf}}Y(\Omega)$ and the vacuum-noise level Ψ_{0s}, we also record the phase-insensitive noise of the signal beam (mode 1) from the NOPA relative to the vacuum-noise level of the same mode, from which we can determine the quantum noise gain G_q. The results for the product $\Delta^2_{\text{inf}}X(\Omega)\Delta^2_{\text{inf}}Y(\Omega)$ derived from measurements as in Fig. 7 are plotted against this quantum noise gain $G_q(\Omega)$ in Fig. 8. The solid theoretical curve drawn in the figure is the result of (32d) of Sect. 1, with the measured normalized frequency $\omega = 0.56$ and loss $L_{\text{overall}} = 0.37$ found from the squeezing traces as discussed in Sect. 3.1. Apart from the discrepancy between the measured loss (0.31) and the loss determined from the squeezing data (0.37), there is otherwise no fitting of theory for these data. The statistical uncertainties in determining the inference variances are very small for a single trace as in Fig. 7; the vertical error bars drawn in Fig. 8 are mainly determined from trace-to-trace fluctuations of the

shot-noise level due to LO intensity fluctuations and drifts in the analysis frequency Ω of the spectral analyzer. The horizontal error bars are also derived from our observations of trace-to-trace fluctuations of the phase-insensitive noise of the signal beam resulting from variations in green pump power. We believe that these error bars fairly reflect the true uncertainties since the quantities $\Delta^2_{\text{inf}}X(\Omega)$, $\Delta^2_{\text{inf}}Y(\Omega)$, the phase-insensitive noise of the signal beam, and the vacuum-noise level are not simultaneously recorded. Clearly from Fig. 8, there is reasonably good agreement between the theory and the experimental data.

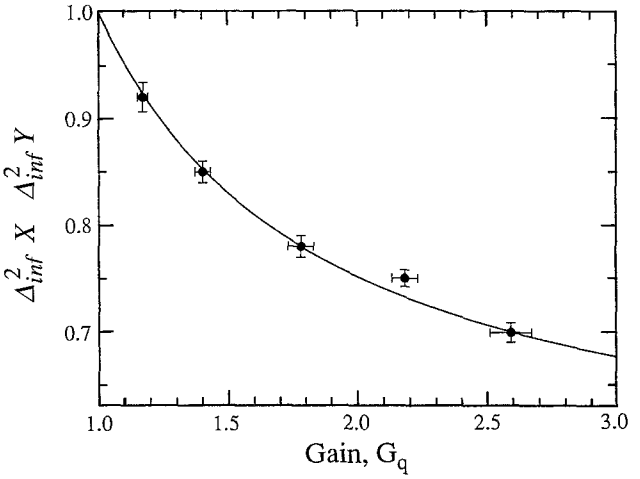

Fig. 8. Product of inference variances $\Delta^2_{\text{inf}}X\Delta^2_{\text{inf}}Y$ vs quantum noise gain G_q of the NOPA. The level of unity is associated with the vacuum-state limit for the signal beam alone. Realization of the EPR paradox requires $\Delta^2_{inf}X\Delta^2_{inf}Y < 1$. The solid curve is the result from (32d) of Sect. 1 with normalized frequency $\omega = 0.56$ and $L_{\text{overall}} = 0.37$ (as in the squeezing trace in Fig. 5)

4 Discussion and Conclusions

In this paper, we have investigated the quantum noise in the output of a nondegenerate optical parametric amplifier (NOPA) and have obtained relatively good agreement between our measurements and the theory of a narrowband NOPA (subthreshold optical parametric oscillator). The quantum correlations of the quadrature-phase amplitudes for the spatially separated signal and idler beams have led to a demonstration of the Einstein-Podolsky-Rosen paradox for continuous variables. The observed variances for the inference of the optical amplitudes of the signal beam from those of the spatially separated idler beam are such that the product of the two inference variances is less than one, which is the lower bound from the Heisenberg uncertainty relation according to EPR. On the other hand, as Bell and others have pointed out [36], the original system discussed by EPR has a perfectly local deterministic description since its Wigner function is non-negative. From (38) of Sect. 2, we likewise find that the Wigner function is everywhere positive for the NOPA. The Wigner function describes the system in an extended position-momentum phase space as opposed to a wavefunction description in either position or momentum space. Thus following the discussion by Bell [36], we see that the Wigner function for either the original EPR gedanken experiment [22] or for the system of the NOPA [20, 21] provides a local hidden-variables description which resolves the EPR paradox. In this sense, our demonstration of the EPR paradox addresses only an apparent nonlocal behavior in a wavefunction description which disappears when we pass to the larger phase-space of position and momentum. In other words, with the aid of the Wigner function, we find that the quantum description for the system of the NOPA as well as for the system originally discussed by EPR is consistent with deterministic local realism. Therefore no paradox exists either in our system or in theirs; the local realism demanded by EPR is not violated in these cases. In more explicit terms, the uncertainty relations of (43a, b) applied locally to either signal or idler fields are not in conflict with the inequality in (49) which refers to cross correlations between these fields. This formal statement is succinctly summarized by the picture of fluctuating field amplitudes in Fig. 1b.

On the other hand, there of course do exist conflicts between a realistic view and quantum theory in many systems with discrete variables [27–31]. To explore analogous irreducible conflicts with continuous variables, we may follow the suggestion by Bell [36] and investigate a system with a Wigner function having negative values, which offers a necessary but not sufficient condition for a violation of a locality inequality. An example of such a system can be found if we go back to (35, 37), where we see that the non-negativeness of the Wigner function for our system comes from the assumed vacuum-state input. If the input to the system instead has a Wigner function with negative values (for example, a single-photon state [9, 38]), then the Wigner function for the output will likewise be negative in some regions. Hence nonlocal correlations between signal and idler beams might exist that could give rise to a true paradox in the modern sense of the Bell inequalities. In this case, the paradox could not be resolved by way of the Wigner phase-space distribution because of its non-positive character; it would not be a true probability distribution that could serve as a hidden-variable distribution. Whether or not there might exist some other type of hidden-variables description based on another one of the infinite set of phase-space quasi-probability distributions for the system just described is unknown and depends upon the successful generalization of Bell inequalities to the case of continuous variables. We hope that our experimental demonstration of the original EPR paradox for continuous variables will serve as a first step toward theoretical and experimental efforts in this direction.

Beyond the relevance of our experiment to these fundamental issues, the correlation properties of the fields generated by the NOPA can also be utilized in precision measurement [2, 15] and quantum communication [16]. As we have demonstrated in this paper, the quantum fluctuations of signal or idler beam individually are quite large and can approach the saturation photon number of the subharmonic field near threshold (for our system, $n_0 \sim 10^4$ with G_q of the same magnitude). On the other hand, the fluctuations for the signal and idler beams are strongly correlated such that when subtracted, the quantities $V^{\lambda}_{\pm}(\Omega) \to 0$ in the absence of loss. Hence if we encode coherent information on the beams, this information can be "shielded" from "unauthorized" detection by the large excess noise in each beam, with the signal-to-noise ratio being very poor for an indi-

vidual beam alone. However, since this excess noise can be efficiently subtracted, the information can be recovered in the dual-beam measurement of $V_{\pm}^{\lambda}(\Omega)$ with signal-to-noise ratio much greater than unity. Of course such a technique can also be employed with correlated classical noises but the signal-to-noise ratio for the dual-beam measurement is then limited by the vacuum noise level from the two beams. Following this lead, we have performed a preliminary experiment in quantum communication similar to the scheme by Hong et al. [16]. With the quantum correlations of the fields from the NOPA, we have observed an improvement in signal-to-noise ratio of 2 dB as compared to the best possible improvement with a classical source.

Acknowledgements. We gratefully acknowledge the contributions of S. L. Braunstein, C. M. Caves, P. D. Drummond, J. L. Hall, K. C. Peng, and M. D. Reid to this research program. Our work was supported by the Office of Naval Research, the National Science Foundation and the Venture Research Unit of British Petroleum.

References

1. (a) L.A. Wu, H.J. Kimble, J.L. Hall, H. Wu: Phys. Rev. Lett. **57**, 2520 (1986)
   (b) L.A. Wu, M. Xiao, H.J. Kimble: J. Opt. Soc. Am. B **4**, 1465 (1987)
2. P. Grangier, R.E. Slusher, B. Yurke, A. LaPorta: Phys. Rev. Lett. **59**, 2153 (1987)
3. R.E. Slusher, P. Grangier, A. LaPorta, B. Yurke, M.J. Potasek: Phys. Rev. Lett. **59**, 2566 (1987)
4. S.F. Pereira, K.C. Peng, H.J. Kimble: In *Coherence and Quantum Optics VI*, ed. by J.H. Eberly, L. Mandel, E. Wolf (Plenum, New York 1989) p. 889
5. P. Kumar, O. Aytür, J. Huang: Phys. Rev. Lett. **64**, 1015 (1990)
6. R. Movshovich, B. Yurke, P.G. Kaminsky, A.D. Smith, A.H. Silver, R.W. Simon, M.V. Schneider: Phys. Rev. Lett. **65**, 1419 (1990)
7. T. Hirano, M. Matsuoka: Opt. Lett. **15**, 1153 (1990)
8. E.S. Polzik, H.J. Kimble: Phys. Rev. Lett. **68**, 3020 (1992)
9. C.K. Hong, L. Mandel: Phys. Rev. Lett. **56**, 58 (1986)
   J.G. Walker, E. Jakeman: Proc. SPIE **492**, 2 (1984)
10. R. Ghosh, C.K. Hong, Z.Y. Ou, L. Mandel: Phys. Rev. A **34**, 3962 (1986)
    Z.Y. Ou, L.J. Wang, L. Mandel: Phys. Rev. A **40**, 1428 (1989)
11. A. Heidmann, R.J. Horowicz, S. Reynaud, E. Giacobino, C. Fabre: Phys. Rev. Lett. **59**, 2555 (1987)
12. O. Aytür, P. Kumar: Phys. Rev. Lett. **65**, 1551 (1990)
13. C.D. Nabors, R.M. Shelby: Phys. Rev. A **42**, 556 (1990)
14. K.W. Leong, N.C. Wong, J.H. Shapiro: Opt. Lett. **15**, 1058 (l990)
15. M. Xiao, L.A. Wu, H.J. Kimble: Phys. Rev. Lett. **59**, 278 (1987); Opt. Lett. **13**, 476 (1988)
16. C.K. Hong, S.R. Friberg, L. Mandel: Appl. Opt. **24**, 3877 (1985)
17. D.C. Burnham, D.L. Weinberg: Phys. Rev. Lett. **25**, 84 (1970)
    S.R. Friberg, C.K. Hong, L. Mandel: Phys. Rev. Lett. **54**, 2011 (1984)
18. B. Yurke: J. Opt. Soc. Am. B **2**, 732 (1985)
19. A. LaPorta, R.E. Slusher, B. Yurke: Phys. Rev. Lett. **62**, 28 (1989)
20. M.D. Reid, P.D. Drummond: Phys. Rev. Lett. **60**, 2731 (1988); Phys. Rev. A **41**, 3930 (1990)
21. M.D. Reid: Phys. Rev. A **40**, 913 (1989)
22. A. Einstein, B. Podolsky, N. Rosen: Phys. Rev. **47**, 777 (1935)
23. N. Bohr: Phys. Rev. **48**, 696 (1935)
24. D. Bohm: *Quantum Theory* (Prentice-Hall, Englewood Cliffs 1951)
25. D. Bohm, Y. Aharonov: Phys. Rev. **108**, 1070 (1957)
26. C.S. Wu, I. Saharov: Phys. Rev. **77**, 136 (1950)
27. (a) J.S. Bell: Physics (N. Y.) **1**, 195 (1965)
    (b) J.S. Bell: *Speakable and Unspeakable in Quantum Mechanics* (Cambridge University, London 1987)
28. J.F. Clauser, A. Shimony: Rep. Prog. Phys. **41**, 1881 (1978) and references therein
29. A. Aspect, J. Dalibard, G. Roger: Phys. Rev. Lett. **49**, 1804 (1982)
30. C.O. Alley, Y.H. Shih: In *Proc. Second Int'l Symposium on Foundations of Quantum Mechanics in the Light of New Technology*, ed. by M. Namiki et al. (Phys. Society of Japan, Tokyo 1987)
    Y.H. Shih, C.O. Alley: Phys. Rev. Lett. **61**, 2921 (1988)
    Z.Y. Ou, C.K. Hong, L. Mandel: Phys. Lett. **122A**, 11 (1987)
    Z.Y. Ou, L. Mandel: Phys. Rev. Lett. **61**, 50 (1988)
31. P. Grangier, M.J. Potasek, B. Yurke: Phys. Rev. A **38**, 3132 (1988)
    J.G. Rarity, P.R. Tapster: Phys. Rev. Lett. **64**, 2495 (1990)
32. R. Ghosh, L. Mandel: Phys. Rev. Lett. **59**, 1903 (1987)
    Z.Y. Ou, L. Mandel: Phys. Rev. Lett. **62**, 2941 (1989)
33. Z.Y. Ou, L.J. Wang, X.Y. Zou, L. Mandel: Phys. Rev. A **41**, 566 (1990)
    Z.Y. Ou, X.Y. Zou, L.J. Wang, L. Mandel: Phys. Rev. Lett. **65**, 321 (1990)
    P.G. Kwiat, W.A. Vareka, C.K. Hong, H. Nathel, R.Y. Chiao: Phys. Rev. A **41**, 2910 (1990)
34. L. Mandel: Phys. Rev. **144**, 1071 (1966)
35. E. P. Wigner: Phys. Rev. **40**, 749 (1932)
36. J.S. Bell: In Ref. 27b, p. 196
    A.M. Cetto, L. De La Pena, E. Santos: Phys. Rev. Lett. **113A**, 304 (1985)
    S.L. Braustein, C.M. Caves: Private communication (1990)
37. (a) M.J. Collett, C.W. Gardiner: Phys. Rev. A **30**, 1386 (1984); **31**, 3761 (1985)
    (b) C.W. Gardiner, C.M. Savage: Opt. Commun. **50**, 173 (1984)
38. H.J. Kimble: In *Fundamental Systems in Quantum Optics*, ed. by J. Dalibard, J.M. Raimond, J. Zinn-Justin (Elsevier, Amsterdam 1992)
39. M.J. Holland, M.J. Collett, D.F. Walls: Phys. Rev. A **42**, 2995 (1990)
40. V.M. Garmash, G.A. Ermakov, N.I. Pavlova, A. Tarasov: Sov. Tech. Phys. Lett. **12**, 505 (1986)
41. Z.Y. Ou, S.F. Pereira, E.S. Polzik, H.J. Kimble: Opt. Lett. **17**, 640 (1992)
42. R.W.P. Drever, J.L. Hall, F.V. Kowalski, J. Hough, G.M. Ford, A.J. Munley, H. Ward: Appl. Phys. B **31** , 97 (1983)
43. H.P. Yuen, V.W.S. Chan: Opt. Lett. **8**, 177 (1983)
    B.L. Schumaker: Opt. Lett. **9**, 189 (1984)
44. The detection electronics were designed by J.L. Hall and fabricated by T. Brown, Joint Institute for Laboratory Astrophysics, University of Colorado, Boulder, CO